ELECTROSPUN BIOCOMPATABLE POLYURETHANES WITH THE ADDITION OF MULTI-WALLED CARBON NANOTUBES

A Thesis

by

Travis Cantu

Submitted to the Graduate School of the
University of Texas-Pan American
In partial fulfillment of the requirements for the degree of

MASTER OF SCIENCE

August 2012

Major Subject: Chemistry

ELECTROSPUN BIOCOMPATABLE POLYURETHANES WITH THE ADDITION OF MULTI-WALLED CARBON NANOTUBES

A Thesis
by
Travis Cantu

COMMITTEE MEMBERS

Dr. Javier Macossay
Chair of Committee

Dr. John Villarreal
Committee Member

Dr. Philip DeLassus
Committee Member

Dr. Elamin Ibrahim
Committee Member

August 2012

ABSTRACT

Cantu, Travis, Electrospun Biocompatable Polyurethanes with the Addition of Multi-Walled Carbon Nanotubes. Master of Science (MS), August, 2012, 52 pp., 10 tables, 26 figures, 43 references, 50 titles.

Three different Polyurethanes (PUs) Lycra®, HydroThane™, and BioSpan®, were electrospun and characterized using Scanning electron microscope (SEM), transmission electron microscope (TEM), Fourier transform-infrared spectroscopy (FTIR), & Raman spectroscopy. Nanofiber composites were made by incorporating MWCNTs at three different concentration 0.1wt% 0.5wt% and 1.0wt% to the three PUs. These samples were characterized and mechanical and thermal test were done. The TEM images showed MWCNT bundling in the polymer matrix at the highest concentration, the FTIR showed shifts in characteristic urethane bands indicating an interaction with the polymer and MWCNTs. Mechanical test showed a decrease in the Young's modulus (E') in most of the composites with the exception of Bio-MWCNTs 0.1wt%. The thermal gravimetric analysis (TGA) did not show an enhancement in the thermal properties of the polymer when the MWCNTs were added. Indicating that the MWCNTs are weakling the stiffness and the thermal stability of the PUs.

DEDICATION

The completion of my doctoral studies would not have been possible without the love and support of my family. My mother, Janie Cantu, my father, Juan Jose Cantu, my sister Monique Y Cantu and my fiancée, Clarisa Vela, whom motivated and supported me by all means to accomplish this degree. Thank you for your love and patience.

ACKNOWLEDGMENTS

I will always be grateful to Dr. Javier Macossay, chair of my dissertation committee, for all his mentoring and advice. From database funding, research design, and data processing, to manuscript editing, he encouraged me to complete this process through his infinite patience and guidance. My thanks go to my dissertation committee members: Dr. Philip DeLassus, Dr. John Villarreal, and Dr. Elamin Ibrahim. Their advice, input, and comments on my dissertation helped to ensure the quality of my intellectual work.

I would also like to thank my colleagues Dr. Faheem Ajamand, Xujun Zhang, John Hamilton, and everyone in our research group for their support in helping me accomplish my goals.

TABLE OF CONTENTS

Page

LIST OF TABLES

Page

LIST OF FIGURES

Page

CHAPTER I

INTRODUCTION

1.1 Introduction

Polyurethanes (PUs) are some of the most versatile polymers known to date. These polymers exhibit a wide range of elasticity's stiffness, and hardness, making them ideal for eraser-soft to bowling ball-hard materials[1].. Polyurethanes also have high tensile strength and melting points making them durable[2]. Recently, much interest in PUs has grown in the medical field, because of their diversity, which includes artificial organs, arteries, skin grafts and ligaments[3].

Polyurethanes typically consist of a hard segment followed by a soft segment; Figure 1 is of a basic linear polyurethane. These covalently bonded chains of long sections of hydrocarbons; which are joined by aromatic or aliphatic hard segments containing urethane or urea groups. The long flexible sections are called the soft section and the urethane/urea group is called the hard segment. In the hard segments, the urethane and urea groups have electrostatic charges on some of the hydrogen, oxygen, and nitrogen atoms[4]. These charged atoms form dipoles which attract another atom of opposite charge, forming a hydrogen bond[5]. The hydrogen bonds formed are of lower strength than covalent bonds in the rest of the chain but are still a factor in forming a strong compound. Therefore, the molecules tend to line up and the hard segments agglomerate in groups where the hydrogen bonding takes place. These molecules are three dimensional the

molecules are not planar but have various groups or atoms protruding and hydrogen bonding takes place in these areas.

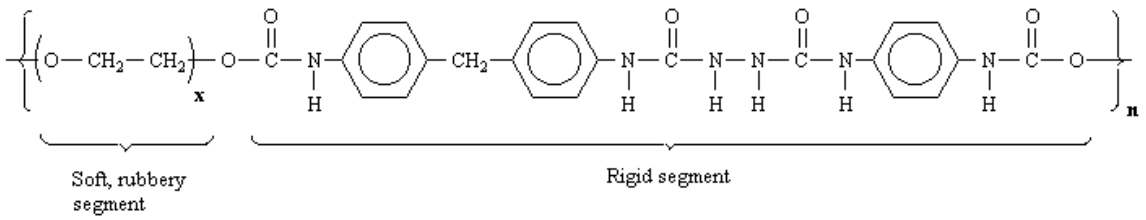

Figure 1 A typical linear PU where the rigid segment (hard segment) Urethane, Aromatic, Urea group. The soft rubbery segment consists of repeating carbon chains[40]

The simple and basic mechanism lying behind the syntheses of PU starts by reacting a hydroxyl-terminated polyester or polyether with an isocyanate[5]. The hydrogen atom of the hydroxyl group is transferred to the nitrogen atom of the isocyanate[4]. This reaction forms what is known as a pre-polymer, this pre-polymer chain is also called as diisocyanate. After the pre-polymer formation, the molecular weight is typically too low to be an elastic polymer; therefore pre-polymers are joined using diols or diamine. This forms the urethane and urea bond respectively in the polymer chain, resulting to formation of PUs. Figure 2 is the synthesis of PUs

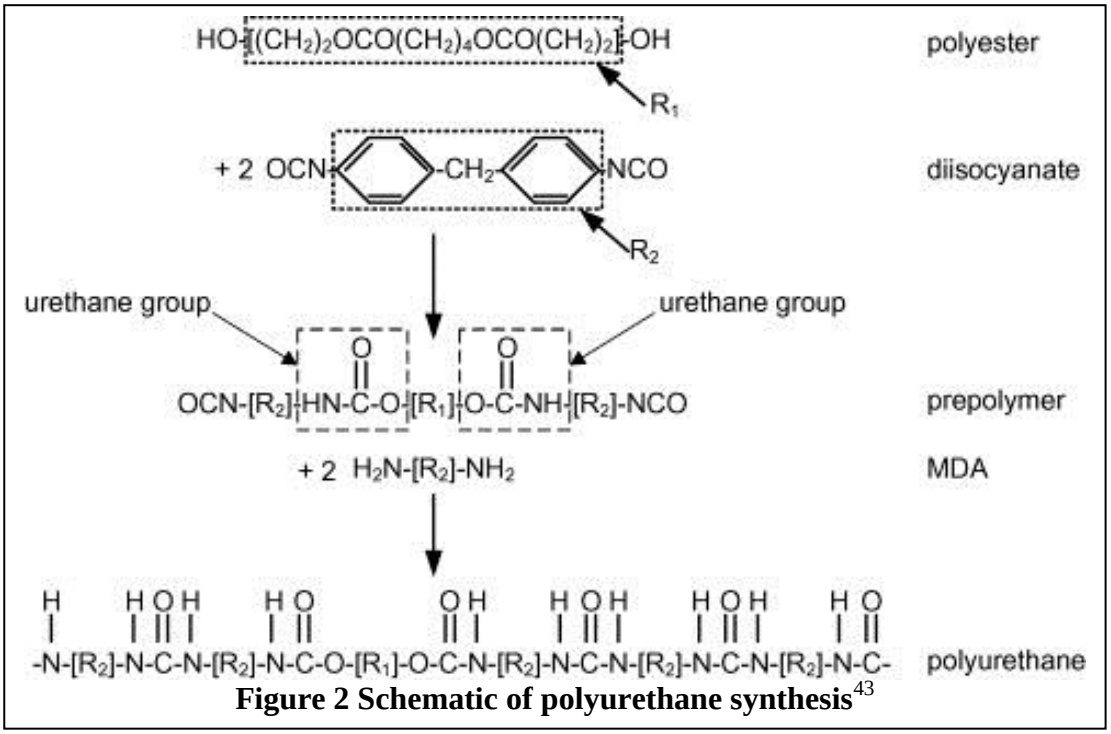

Figure 2 Schematic of polyurethane synthesis[43]

1.1.1 Methods of developing nanofibers

In the nanotechnology field, many methods have been developed to produce nanofibers, which have diameters smaller than 1000 nm. These nanofibers are of interest because they have potential applications in various medical and non-medical fields. The methods that have been developed in order to produce these nanofibers include centrifugal spinning,melt blowing , hydrothermal, and electrospinning. Centrifugal spinning uses high centrifugal forces to produce nanofibers; in this process, a polymer solution is forced out from a tiny opening in the form of nanofibers[6]. Melt blowing is a process where fibers are produced in a single-step by extruding a polymer through an orifice die and drawing down the extrudate with a jet of hot air[7]. The drag of the hot air on the surface of the polymer melt causes the polymer, under optimal conditions, to elongate into a fiber[8]. This method is used mostly commercially. The hydrothermal method is a temperature dependant technique widely applied to prepare various nanofibers due to high reactivity of reactants and excess of pressure created during the process, this method is easy to control and causes less air pollution. The method that will be discussed in detail is electrospinning, which is the most popular and easiest method.

1.2 Electrospinning

1.2.1 Electrospinning History

In the early 1900s J.F. Cooley and W.J. Morton patented the elctrospinning process[9]. Cooley patented a set-up that used electrodes to direct the electrospinning jet onto a rotating collector[9]. In the 1930s Formhals invented many different set-ups that would electrospin yarn fibers without the use of spinnerets[9]. In the fiber industry one key factor is the amount of output, and, electrospinning, compared to the conventional methods of producing fibers was not as

efficient, for this reason there was very little research done on this method[9]. However, in the 1990s the electrospinning process began to resurface and in the early 2000s increased research in biomedical equipment and prosthesis found electrospinning to be a very useful technique, due to the production of high yields. In the recent years, this process has grown in popularity because of cost, convenience and multiple applications. Much research is still being done on different conditions of electrospinnig, such as controlling diameter size, morphology and structure of the nanofibers. The ability to control these features makes electrospinning a valuable technique. The potential applications of the material changes dramatically when the diameter of the polymer fiber is decreased from micrometer to nanometer level, as this increases many different characteristics of the fiber, such as a larger surface to volume ratio, flexibility in surface functionalities, and increased mechanical performance[10]. These characteristics make electrospun nanofibers ideal for many applications in the medical fields, in protective clothes, as biosensors, biochips, artificial valves, tendons, ligaments, and muscle replacement..

1.2.2 Electrospinning Process

Electrospinning is a process that produces fibers with diameters ranging from 40-900nm. These small diameter fibers produce high surface area to volume ratio, and high length to diameter ratio[11]. These characteristics play an important role in the many applications of electrospun nanofibers. In this process, a polymer solution (typically) is placed in a syringe, and an electric field ranging from 5-30kV[10] is applied, with a ground or opposite polar potential a short distance away attached to the target. This creates an electric charge on the polymer solution being ejected from the syringe, which is attracted to the ground or opposite polarity forming the Taylor cone on the nozzle of the syringe. There is a critical value in the electric field in which

repulsive forces overcome the surface tension forces[11] . The polymer nanofibers are formed as the solvent evaporates from the jet, solidifying the polymer and landing on the target. Figure 3 is an image of a typical electrospinning setup.

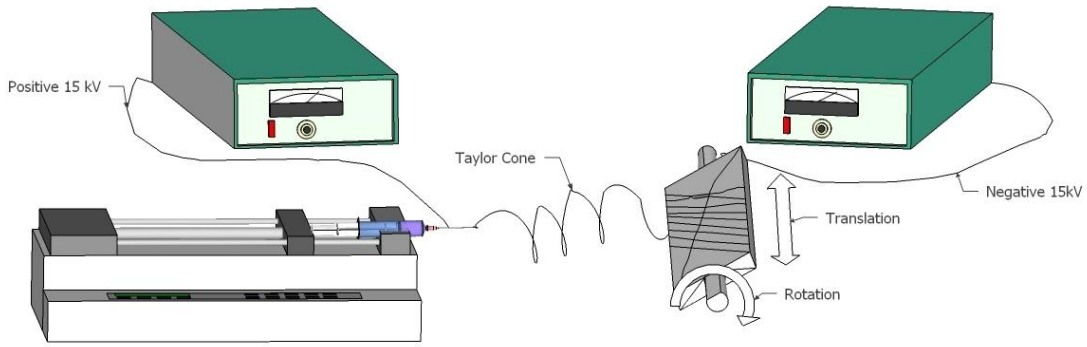

Figure 3 Schematic of electrospinning setup used in experiments

1.3 Ligaments & Tendons

Ligament comes from the Latin word ligare which means band or tie, and tendon also comes from a Latin root, tendere which means to stretch[12]. Ligaments are therefore defined as a tough fibrous band of tissue connecting the articular extremities of bones or supporting an organ in place[12]. Tendons are a tough cord or band of dense white fibrous connective tissue that unites a muscle with bone and transmits the force which the muscle exerts[12]. Ligament and tendon tears are becoming more and more common ranging from adolescents to elderly people. The most common place for a torn ligament is in the knee, it is estimated that 100,000 anterior cruciate ligament (ACL) reconstructive surgeries are done annually in the United States alone[13]. The most common tendon injury occurs at the Achilles. Most of these injuries are related but not limited to sports, while many of these injuries occur in elderly people based on wear and tear, being more

difficult to repair these types of injuries in elderly people. If a tendon or ligament is torn, surgery in most cases is inevitable. One of the most common surgical procedures is where a graft is taken from another ligament or tendon of the patient (autograft) or from a cadaver (allograft), then the graft is placed and screwed in place. In the case of an ACL tear, the graft is taken from the patellar tendon, this tendon is then used in place of ACL; a screw is drilled through the tibia where the ACL would be and into the femur. The graft is then passed through the hole and screwed in place. Figure 4 shows where the replacement will be screwed in. These procedures are complicated and require a graft to be taken from another part of the body. Unfortunately, this procedure has a long healing process.

Figure 4 This is how a typical ACL replacement is done a hole is drilled from the tibia in to the femur, the replacement is then screwed in[41].

Many researchers have begun to focus on developing a method that has a quicker healing process and that does not require a graft to be taken from the patient. One such method is incorporating electrospun nanofibers as a prosthetic tissue for ligaments and tendons. These nanofibers have the potential to be very flexible and durable, and at the same time accepted by

the body. Polyurethanes, which are biocompatible and mechanically strong, are becoming more common in this type of field.

Tissue engineering is a growing field in which it involves the *in-vitro* seeding and attachment of human cells onto a scaffold[14]. Tissue engineering approaches this reconstruction by evoking the general principle of porous scaffolds that deliver bio-factors (cells, proteins, signaling factors) to generate natural tissue[15]. Scaffolds must meet certain requirements, and must meet a specific fit with very complex 3-D structures. The scaffold requirements are very specific, providing structural support and maintaining mechanical integrity until the tissue begins to form. In most cases, biodegradability is an important factor, since the scaffold should degrade and be absorbed by the host tissue in order to avoid the need for surgery to remove the scaffold. The degradation must coincide with the rate at which the tissue will regenerate, so while the cells are regenerating and forming their own natural matrix, the scaffold is able to provide structural integrity until the natural tissue can take the mechanical load. There are many types of scaffolds and they are made of different materials, which include natural polymers and synthetic ones. Currently, biodegradable and biocompatible polymers are being studied in the medical field.

1.4 Carbon Nanotubes

1.4.1 Properties of Carbon Nanotubes

The Young's modulus (E') of a material is the first step to knowing how to use the material as a structural element for various applications[16]. The Young's modulus is the ratio of the stress to strain; this can be used to predict the elongation and compression of an object. In this respect, the Young's modulus is directly related to the inter-molecular attraction between

similar molecules of a solid. Moreover, in the case of covalently bonded solids, it is the shape of the potential energy of a pair of atoms as a function of the inter-particle separation that determines the elastic properties of an ideal crystalline solid[16]. Carbon nanotubes (CNTs) have high aspect ratio which in turn reflects excellent mechanical properties. The natural carbon-carbon sp^2 hybridization is expected to give CNTs very high strength and modulus[17]. There are many types of CNTs but all fall into two main categories, single-walled CNTs (SWCNTs) and multi-walled CNTs (MWCNTs). The difference between the two is that SWCNTs have a graphene sheet rolled onto itself, forming a tube, whereas MWCNTs have a graphene sheet rolled onto itself many times creating different layers, this can be seen in Figure 5. Studies showed that the Young's modulus for CNTs is as high as graphite (approximately 1 TPa) and is slightly higher for small SWCNTs[16] It is expected that the mechanical properties of CNTs will be reflected in polymer composites[17].

1.4.2 Production of Carbon Nanotubes

In 1991 Iijima published work on transmission electron microscopy, that showed observations of elongation and concentric layered microtubes made of carbon atoms[18]. In 1996The Noble prize was awarded to Harry Kroto, Robert Curl, and Richard Smalley in Chemistry for the discovery of a nanometer spherical molecule composed entirely of carbon atoms[18], which were named fullerenes. Up until this point, these elongated concentric layered microtubes were considered as filamentous carbon[18]. These microtubes would come to be known as carbon nanotubes (CNTs). There are various methods used to produce CNTs, some of which include sublimation of carbon under an inert atmosphere, an electric arc discharge process, or the solar technique[18] There are also chemical methods that can be used to synthesize CNTs, such as the catalytic decomposition of hydrocarbons method[18].

The carbon arc-discharge method is a high temperature process, which produceses CNTs as well as fullerenes. This is probably one of the simplest methods for synthesizing CNTs, and is the preferred method when producing large scale amounts. In this method, an arc is ignited between two electrodes in a gaseous background, where the arcing evaporates the carbon and while it cools and condenses, some of the product forms as filamentous carbon on the cathode. Iijima claimed that this filamentous product were indeed multi walled carbon nanotubes, and the optimization of metals being included in the anode led to the growth of single-walled nanotubes[18]. Other methods are more complicated and not preferred, because of cost and efficentcy. Figure 5 is a schematic of arc- discharge system.

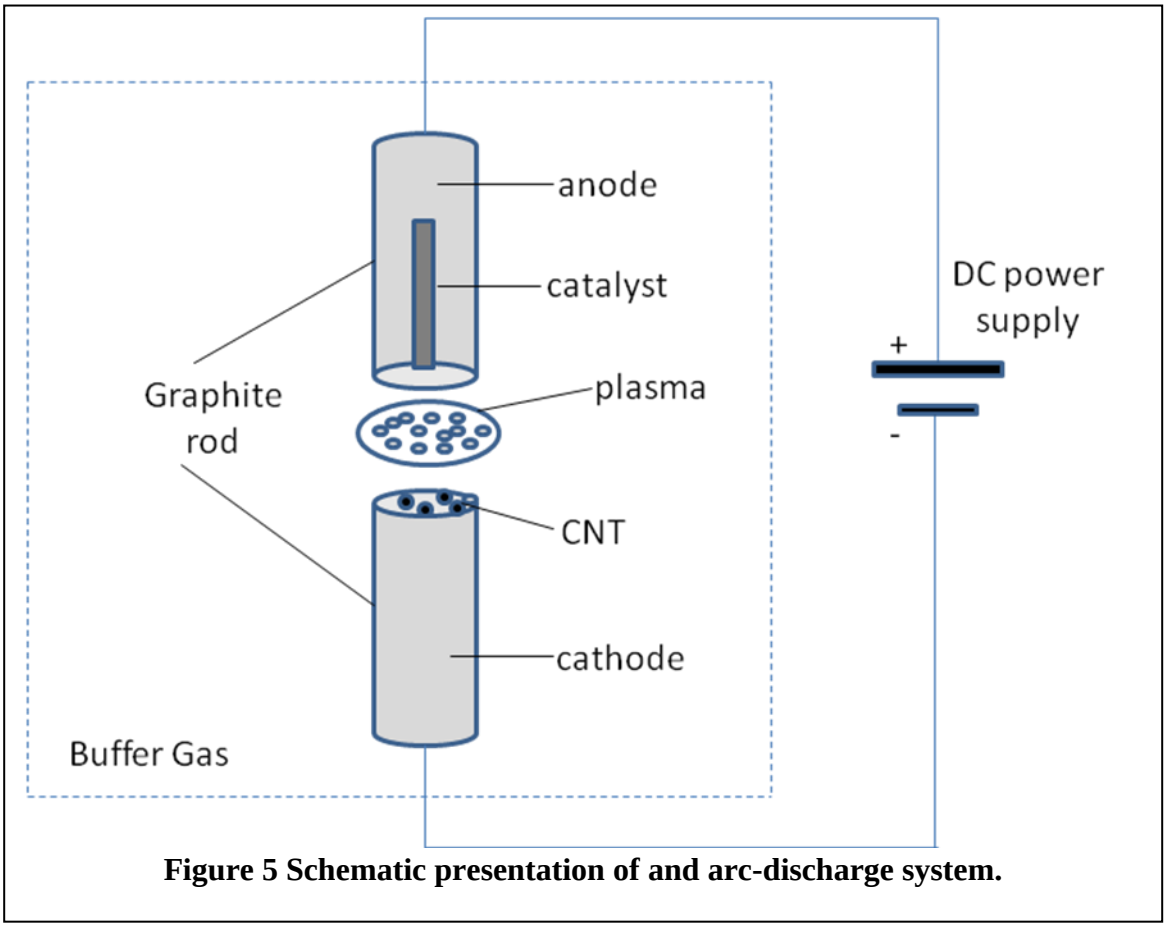

Figure 5 Schematic presentation of and arc-discharge system.

1.4.3 Dispersion of Carbon Nanotubes

One obstacle that is challenging researchers in CNT reinforced composites is the even dispersion of the CNTs and the orientation and alignment, which in the matrix leads to agglomeration and bundling. Theoretically, in order for the CNT composites to show superior properties, the CNTs should be dispersed and perfectly aligned in the matrix. Research has shown that CNT composites show some improved properties, but many fall short of the theoretical predictions due to uneven dispersion in the polymer matrix, which would lower the load transfer efficiency[19]. Many different methods have been produced in an attempt to disperse CNTs in the matrix. One of these methods is to disperse CNTs through ultra sound sonication and high speed shearing, resulting in a convenient and simple approach for high dispersion[20]. Additionally, surfactants can be used as a dispersing agent to improve the dispersion in the polymer CNT composites. A study used polyethylene-8-lauryl, a non-ionic surfactant, as a processing aid for epoxy composites[21]. The strong interactions between the carbons of the CNTs and the hydrophobic segment of the surfactant via van der Waals forces, promoted that CNTs aligned and stayed dispersed within the polymer matrix[21]. This study also showed that the CNTs dispersed in the surfactant improved the thermal-chemical properties of the composite. Other research showed that compatibilizers and polymer-assisted melt blending also helped disperse CNTs[21].

1.5 Research Objective

The objective of this project is to determine the electrospinning conditions for three PUs, Lycra®, Hydrothane™ and BioSpan®. Once the conditions for electrospinning are determined, three different concentrations of MWCNTs will be incorporated into the polymers to enhance the

mechanical properties.. In order to disperse the MWCNTs, the process of ultra sound sonication will be utilized, asthis method has shown that this is an efficient process for de-bundling CNTs. The optimum conditions for sonication will have to be determined experimentally. Subsequently, these samples will be electrospun to form nanofibers containing MWCNTs. Several methods will be used to investigate the samples, including scanning electron microscope (SEM), transmission electron microscope (TEM), Fourier Transform Infrared Spectroscopy FT-IR and Raman spectroscopy. The SEM will be used to image the electrospun nanofibers. From these images, the morphology and fiber diameters will be determined. The TEM images will be used to determine how the MWCNTs are aligned within the polymeric nanofibers, while FT-IR and Raman spectroscopy will be used to examine the chemical structure of the nanofibers and its effect on shifting functional groups and vibrations occurred due to the presence of graphitic and disorder bands of MWCNTs. Mechanical analysis of the three different PUs, Lycra®, Hydrothane^{TM}, BioSpan® composites containing MWCNTs will also be conducted. This test will determine the mechanical properties of the polymer nanofibers containing MWCNTs, in order to establish their effect in the polymeric matrix. Further, thermal gravimetric analysis will be used to determine the thermal stability of the pristine electrospun nanofibers and compare it against the nanofibers containing MWCNTs The ultimate goal of this research project is to use these reinforced polymer fibers as scaffolds for artificial ligaments and tendons. To our knowledge, no work has been done in this field by using these polymer composites reinforced with MWCNTs.

CHAPTER II

MATERIALS AND METHOD

2.1 Materials

Lycra® was kindly obtained from Invista (Whichita Kansas) HydroThane TM (HydroThane ^{TM} AR 25-93A) was purchased from Cardiotech International Inc. (Wilmington Massachusetts), and BioSpan® Segmented Polyurethane was purchased from PTG Medical LLC (Berkeley California) at a concentration of 24 ± 2wt/vol% in DMAC. BioSpan® was dried, so that the DMAc could be removed forming a solid polymer. Tetrahydrofuran 99+% (THF), N,N-dimethylformamide 99.8% (DMF) and N,N-dimethyacetamide 99+% (DMAc) were purchased from Sigma-Aldrich and used without any further purification. Multi Walled-Carbon Nanotubes were acquired from Bayer Material Science Baytubes C150HP®. The CNTs have a C-Purity of ≥95 wt% with a manufacturer reported outer diameter of ~13nm and inner diameter of ~4nm and length of >1μm.

2.2 Electrospinning Conditions

The optimum concentration for HydroThane TM was experimentally determined to be 20% w/v, when using a lower concentration the fibers would not form. The flow rate was based on the solvents used to dissolve the polymer, in the case of HydroThane TM a 50:50 mixture of

THF:DMF was used. From previous research polymers electrospun in this solvent mixture work best at a rate of 0.05ml/min, and this was also the case for HydroThane ™. At this rate there was very little dripping and fibers were observed immediately on the target. The distance was set at 23cm as the initial distance; the distance was kept constant for the initial electrospinning trials. The voltage was set at 15 kV for the positive charge and 15 kV for the negative charge, the positive charge was attached to the needle and the negative was attached to the target.

Lycra® and BioSpan® both dissolved in DMAc with a rate of 0.01ml/min. At this rate, the samples were dry enough and nanofibers were produced. The distance for both was 23cm from tip to collector, and the voltage set up was the same as HydroThane ™. The electrospinning conditions are listed in **Error! Reference source not found.**.

Table 1 Electrospinning conditions

Polymer	Concentration (wt/vol%)	Solvent	Distance (cm)	Rate (ml/min)	Voltage (kV)
Lycra®®	7.5	DMAc	24	0.01	15
BioSpan®	10	DMAc	24	0.01	15
HydroThane ™	20	THF:DMF	24	0.05	15

2.3 Sonication

The MWCNTs were sonicated in the solvent used to dissolve the polymer for an 1 hr, the polymer is not sonicated because if sonicated long enough the polymer could be denatured and will lose its physical properties, which in turn will results in low molecular weight of the polymer. YOU ARE CHOPPING OFF YOUR WRITING AND FLOW OF IDEAS BY HAVING EXTREMELY SHORT SENTENCES. After sonicating in an ice bath for 1hr the polymer was added at the same concentration as electrospun without the MWCNTs. The sample

was vortexed for 24hrs, then electrospun in the same manner as previously done for pure polymers. The samples containing HydroThane ^{TM} were sonicated in DMF initialy, after 1 hr of sonication THF was added. This was done to prevent THF from evaporating during sonication. MWCNTs were added in three different concentration 0.1wt%, 0.5wt%, and 1.0wt% with respect to the polymer. Conditions are listed in Table 1.

2.4 Scanning Electron Microscope (SEM)

The samples were coated with palladium with the use of a Denton Vacuum Desk II Sputter and etch unit. The samples were coated for 120 sec at 45 mA. Further on, the samples were imaged in a EVO LS10 (Carl Zeiss Microscopy)

2.5 Fourier Transform Infrared Spectroscopy (FTIR)

FTIR spectra of the nanofibers were obtained and used to characterize the polymers and their interactions with the MWCNTs. The electrospun samples were run as fibers mats through KBR window, and the spectra were determined using a Bruker FTIR (IFS 55) form 4000-600 cm^{-1} with an 8 cm^{-1} resolution and 32 scans.

2.6 Raman Spectroscopy

Raman Spectroscopy was used to complement FTIR spectroscopy. Raman spectroscopy spectra were acquired using a Bruker (Senterra) from 4000-600 cm^{-1} with 10mw power, 50

integrations, 2 co-additions and 50X magnification. The samples were run as fiber mats on glass slides. An average of 5 trials were taken for samples containing high concentration of CNTs, which was necessary to have low noise and variation free spectrum of the samples.

2.7 Mechanical Testing

The mechanical tests were done using an Instron 5943 on 10 dog bone shaped samples cut from electrospun fiber mats with dimensions 6.2 X 18.6 mm. The samples were placed within the grips andstrained until failure. The test load is 50N and an extension rate of 10 mm/min.

2.8 Thermal Gravimetric Analysis (TGA)

TGA was used to determine the on-set decomposition temperature of the samples. The comparison between the electrospun polyurethanes and the composite nanofibers containing MWCNTs allowed to determine the effect of the nanotubes in the polymeric matrix. Samples were investigated in a TGA 7 (Perkin Elmer) and heated from 20 to 800 ^{o}C at a rate of 10.00 ^{o}C/min under continuous purge of nitrogen at a flow rate of 20 ml/min.

CHAPTER III

RESULTS AND DISCUSSION

3.1 Production of nanofiber mats

3.1.1 Electrospinning Conditions

There are many factors that play an important role in electrospinning, these include solvent, voltage, tip to collector distance, rotational speed, viscosity, temperature and humidity[22]. A study used ratios of two different solvents ethanol and DMF in PVP and determined how the fiber diameters were affected[23]. In ethanol alone the polymer produced smooth nanofibers, when the solvent was a 50:50 mixture of ethanol and DMF at 4 wt% the nanofiber diameter was as small as 20 nm[23]. When the solvent mixture was increased from 4 wt% to 8 wt% the nanofiber diameter increased from 20 to 50nm without significant change in the size distribution[23]. This is just one example there are several studies that report how solvent affects the electrospinning process, most of the information in these studies are related to morphological changes due to viscosity and electro conductivity.

The needle to collector distance has been reported from 7 cm to 50 cm in different experimental setups, but not all report on the effects of the separation from needle to the collector. It was reported in an experiment of polystyrene, that as the collector distance increased from 7, 10, and 15cm the diameter of the nanofibers decreased[22]. The contrary is shown where

beads are present as the distance increases so do the beads[22]. This shows that more research needs to be done in order to clarify the effect of the needle to collector distance.

A study done on voltage tested poly (acrylonitrile) PAN at different concentrations and different voltages, and the study concluded that there was no significant fiber change in the diameter or the morphology[24]. This is also consistent with similar studies so it can be concluded that voltage plays a factor but not a large role in electrospinning.

A study observed that the needle diameter affect is very limited on the electrospinning process. One research group electrospun poly(lactide-co-glycolide) and used a range of needle diameters, from 0.029 to 0.059cm, while all the other conditions will be remained constant[25]. There results showed that as the diameter of the needle decreased so did the fiber diameter from 250 to 125nm[25]. However, in a paper published by our group that showed the needle gauge did not affect the diameter size, and did not really affect any aspect of the electrospinning[26]. These results lead to believe that some work should still be done, on how the diameter of the needle affects the electrospinning. However, for now this factor will be considered as a variable that does not play a major role in electrospinning.

The effects of the environment, such as humidity, have been studied by researchers, and it is shown that humidity can affect the electrospun fibers. The study showed that at elevated humidity the fibers were pours[22]. No definite comparison has been made with experimental data, some researchers suggest that the humidity coupled with other conditions affects electrospinning. These parameters need to be studied in more detail before any definite answer can be made[22].

Many literature sources report polymer concentrations ranging from 1 to 40%, but most are typically less than 30%[22]. One source reported that as the initial Nylon 6 concentration increased from 10 to 25% the fiber diameter increased from 80 to 250 nm[27]. This is a predicted trend and is observed by many researchers[22]. This has also been observed by research done in our group.

By increasing the flow rate, research has shown it tends to increases the fiber diameter[22]. It is shown that flow rate affects diameter size and morphology, there is nothing conflicting about this research and no further studies have been done on flow rate.

Research shows a strong dependence on viscosity for fiber morphology. Nearly all research shows that by increasing the zero-shear viscosity, whether by molecular weight or by increasing concentration, will increase the fiber radius[22].

The studies done on these conditions play a major role in determining the electrospinning conditions for Lycra®, BioSpan®, and HydroThane™ ™, and will be considered during experimentation.

The electrospinning conditions for the three polymers were determined by trial and error methods. From the many factors mentioned above four parameters were adjusted in order to determine the best electrospinning conditions (i.e., voltage, tip to collector distance, flow rate, and viscocity/concentration).

3.1.2 Incorporation of Multi-Walled Carbon Nanotubes

The use of multi walled carbon nanotubes (MWCNTs) in polymer composites is becoming more and more common due to the physical characteristic of MWCNTs. Carbon nanotubes have high aspect ratio which only contain few defects[17], MWCNTs also have low density which makes them ideal candidates for polymer reinforcement composites. Research has shown that CNTs have improved mechanical properties and thermal properties of polymer composites. The main issue that researchers run into is the uniform dispersion and orientation alignment of CNTs in the polymer matrix. Many methods have been developed such as the use of DNA to help keep the CNTs dispersed and also the use of surfactants was done[28,20] .

Interest has increased to use DNA as a vehicle to separate and align CNTs, the ideal DNA length should be in the order of micrometers[28].Researchers now are attempting to determine the binding affinity of DNA to many substances using a method called phase display. One research article found that short oglionucliotides have repeating sequences of gunanins and thymines could wrap around a CNT in a helical manner[28]. There is still much work that needs to be done on using ssDNA to disperse CNTs, i.e. studies need to be done on the effect of CNT diameter and chirality, and which sort of ssDNA is best for aligning and dispersing CNTs.

A study done by our group on the use of surfactants to aid of dispersion of CNTs showed no change in properties of nanotubes[29]. The study used Triton X-100 a nonionic surfactant, and CNTs were sonicated for two hours in the surfactant, then the polymer was added. When the samples were compared to those without the surfactant, and no notable difference was noticed in

the thermal test. From our results, it was determined that the use of a surfactant was not something the group was willing to completely pursue.

3.2 Lycra® (L)

3.2.1 SEM Images

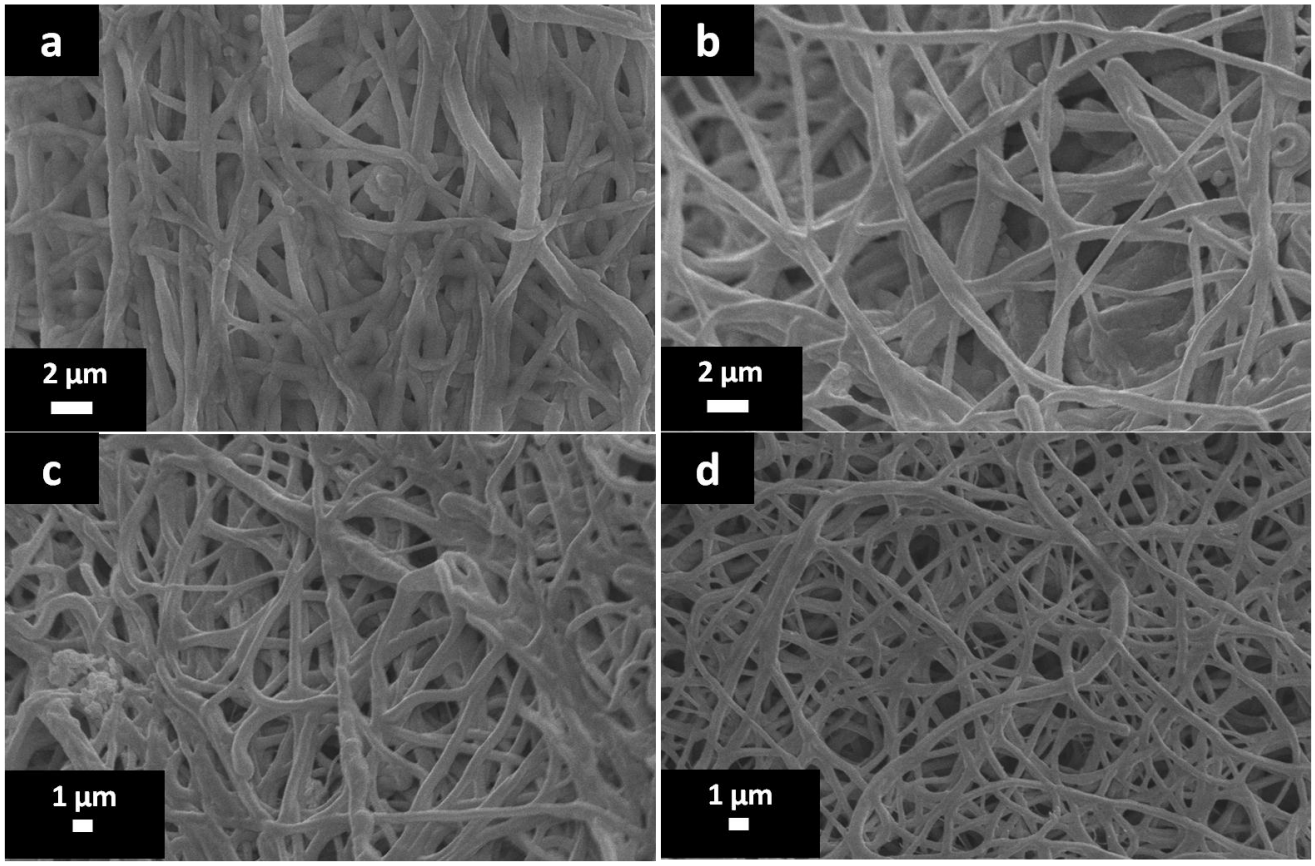

Figure 6 SEM images of Lycra® (L). (a) electrospun L, (b) L-MWCNTs 0.1 wt%, (c) L-MWCNTs 0.5 wt%, (d) L-MWCNTs 1.0 wt%.

From Figure 6 the electrospun fibers are randomly aligned.From the images very little beading is observed, showing that the electrospinning conditions are optimum to obtain defect free nanofibers. The SEM method provides valuable information on the morphology and structural compostition on the nanofibers obtained[30].

3.2.2 TEM Images

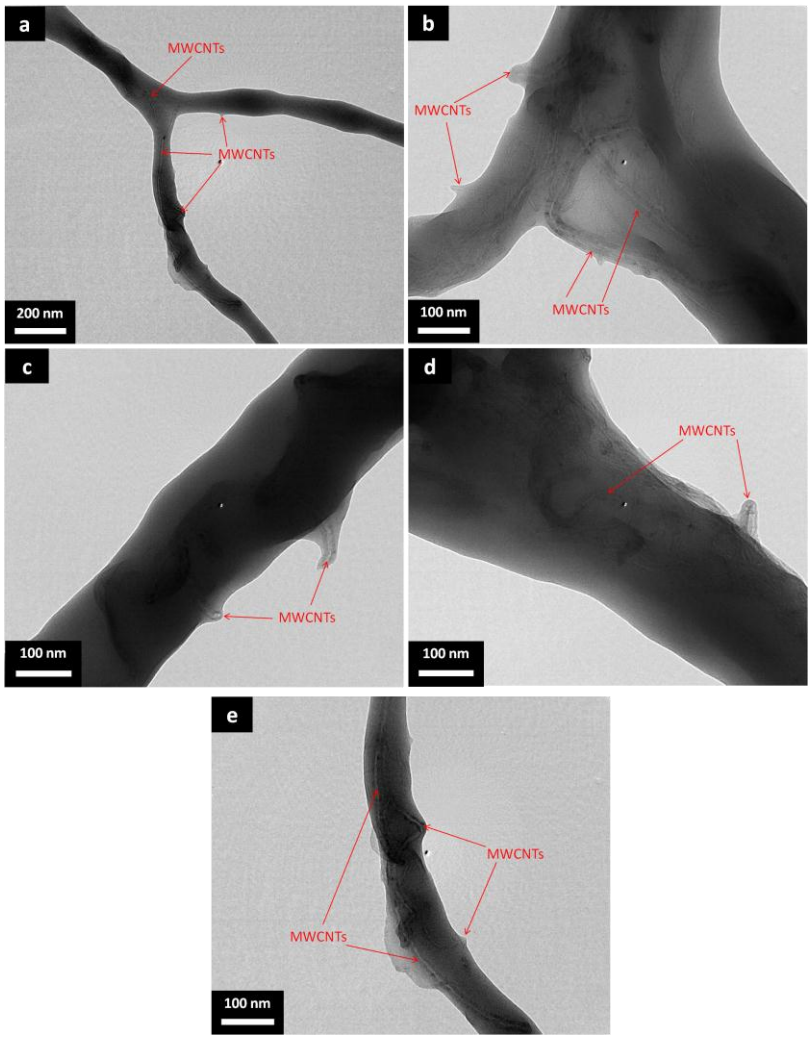

Figure 7 TEM images of L: (a-e) are of L-MWCNTS 1.0 wt% at different areas of the polymer.

The TEM images of L-MWCNTs 1.0 wt% show the MWCNTs embedded in the polymer matrix . These images show that the MWCNTs are in no particular arrangement, being randomly dispersed in the matrix. In certain areas, MWCNTs are slightly bundled and some are protruding out of the polymer matrix. Research published by C. Brower and coworkers showed similar results, also noting that a layer of polymer was coating the protruding MWCNTs[31].

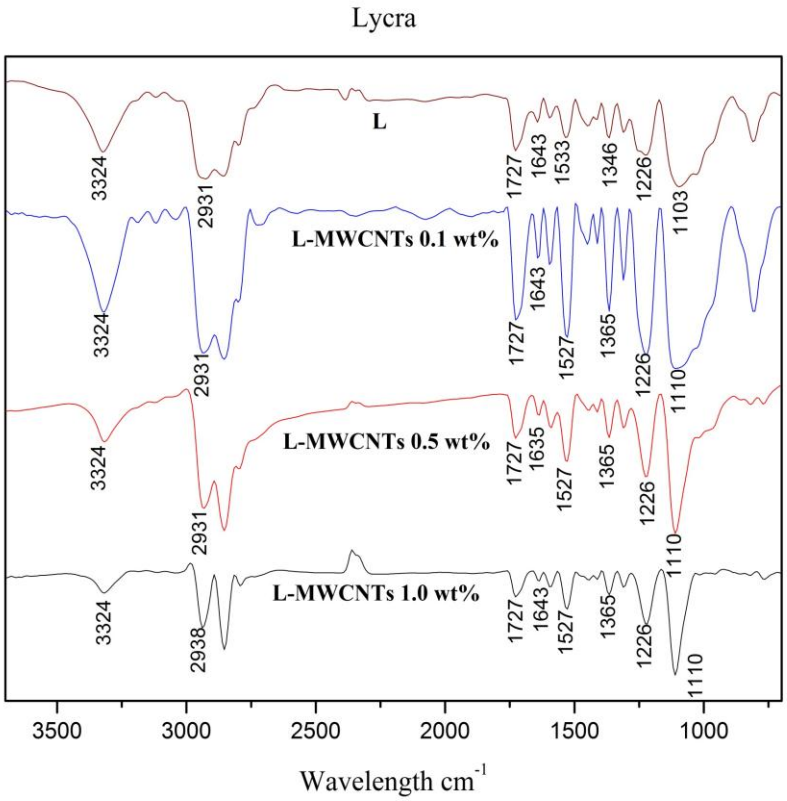

Figure 8 FTIR of L and L-MWCNTs

3.2.3 FTIR Spectroscopy

From Figure 8, the peak at 3324 cm^{-1} is seen in all of the samples and is due to -NH end groups; as the concentration of the CNTs increase, the intensity of the band decreases, which may be due to the CNTs interacting with the end groups. The band at 2931 and 2800 cm^{-1} is due to C-H aliphatic stretching from methylene and ethylenediamine[32]. One thing that is observed is the intensity of 2931 and 2800 cm^{-1} flip as the concentration of the CNTs is increased and it becomes more defined as seen in the sample contain 1.0% MWCNTs. Therefore, the C-H asymmetric stretching from the Lycra® are interacting with the MWCNTs. The carbonyl peak from the urethane is observed at 1727 cm^{-1} the peak is not shifted, but the intensity of the peak is initially increases in L-MWCNTs 0.1wt% and then decreased as the concentration of CNTs

increases. This increase in intensity may be due to a change in dipole where the MWCNTs are interacting with the rigid segment of the PU. As the concentration increases the MWCNTS start to interact with themselves and less with the polymer therefore decreasing the dipole change and the intensity of the FTIR peaks. The bands at 1643cm^{-1} and 1533cm^{-1} are due to N-C=O urea stretching and N-H in-plane bending respectively{ref}. The band at 1533cm^{-1} is shifted to 1527cm^{-1} once the MWCNTs are introduced, due to π-π interactions with the N-H and the MWCNTs The bands at 1226cm^{-1} and 1110cm^{-1} are related to O-C-O-NH of the urethane and C-O-C bonds[33]. As the concentration of MWCNTs increases, the bands at 1226cm^{-1} & 1110cm^{-1} narrows , which could be attributed to to masking of these groups, the change in shape maybe due to a decrease in intensity of the bands attributed to the interaction of the polymer with the MWCNTs. The band at 800cm^{-1} is observed in the pure Lycra® and in the sample containing 0.1% MWCNTs, but once the concentration is increased to 0.5wt%, the band almost completely disappears, and at 1.0wt% it isn't visible.

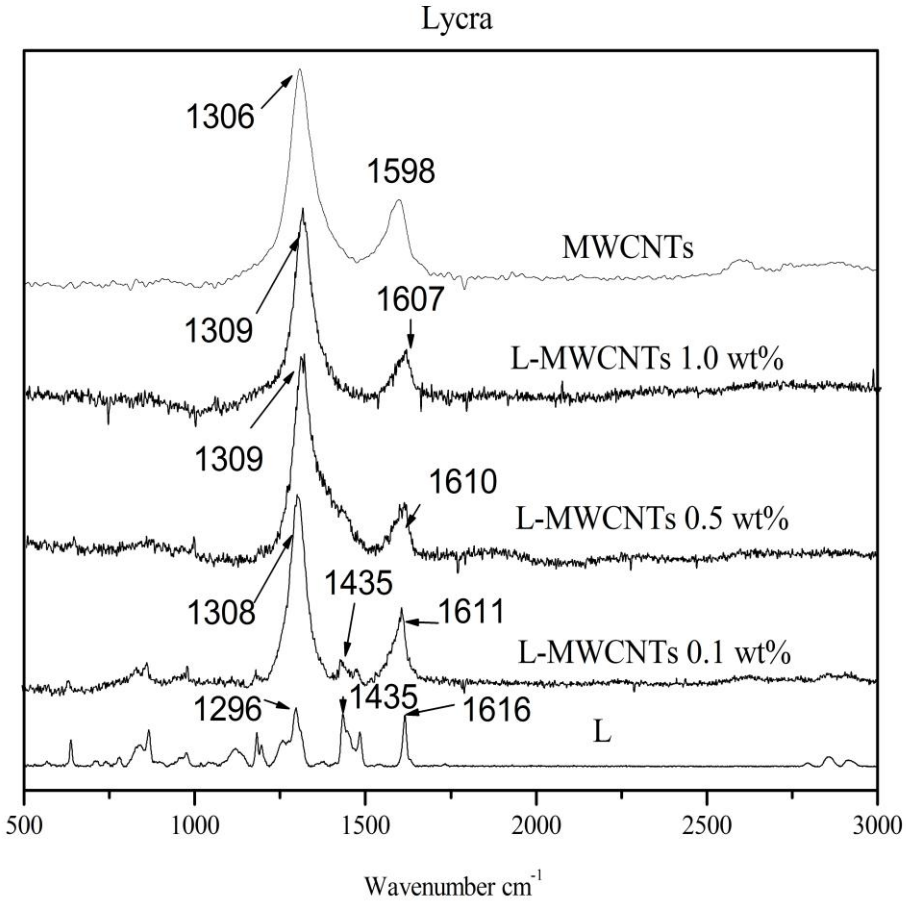

Figure 9 Raman Spectroscopy of L and L-MWCNTs

3.2.4 Raman Spectroscopy

The spectra in Figure 9 of electrospun L has peaks at 1435, and 1616 cm^{-1} which are assigned to the aromatic C=C stretching, while the peak at 1296cm^{-1} is due to aromatic ethers. In spectra L-MWCNTs 0.1 wt%, the peak at 1435cm^{-1} is significantly decreased and the peak at 1296 cm^{-1} is masked by the presence of the D-band at 1308 cm^{-1} [34]. From spectra L to L-MWCNTs 0.1 wt%, there is a shift from 1616 to 1611 cm^{-1}, which is in the region of the G-band, a characteristic peak of CNTs[34]. From Figure MWCNTs bulk show the D-Band at 1306 cm^{-1} and the G-band at 1598 cm^{-1}. The G-band is known as the graphitic band, in this mode the atomic displacement occurs along the circumferential direction[35]. The D-band is known as the disordered band which is related to the longitudinal movement of electrons within the MWCNTs

structure[35]. Some research suggests that in MWCNTs, the G-band is masked by the appearance of a second D-band known as D'-band[36]. The intensity of the D-band is higher than the G-band due to the multiple layers of the MWCNTs[37], which means that there are more disordered bands than graphitic bands in MWCNTs. In spectra L-MWCNTS 0.5 wt% and 1.0 wt%, the 1435 cm^{-1} peak is completely masked and the band atthe 1600cm^{-1} range was shifted down. The broadening of the G-band shows that as the concentration is increased, the MWCNTs are less dispersed[34].

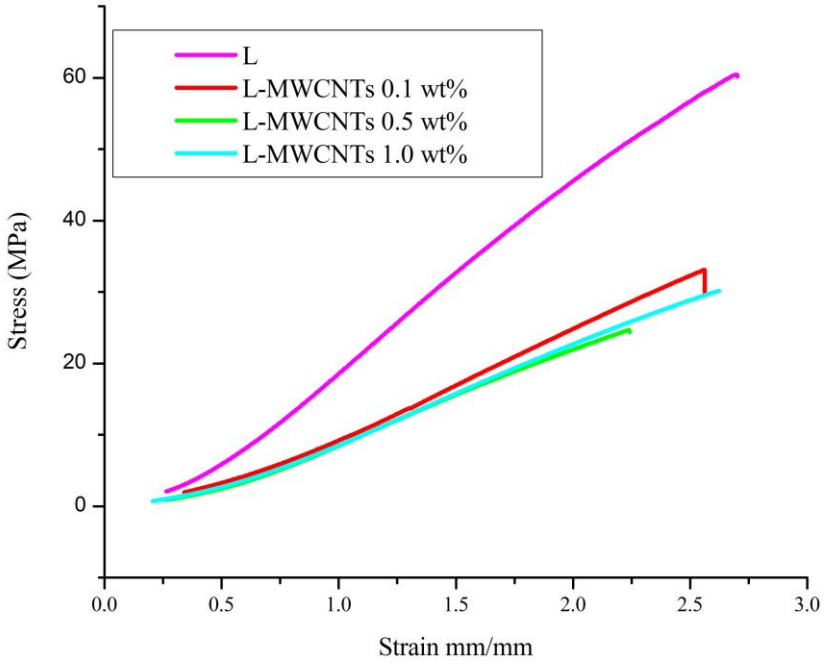

Figure 10 Mechanical Test of L and L-MWCNT composites.

Table 2 Results from mechanical tests (L)

Polymer	Tensile Stress MPa	Strain mm/mm	Young's Modulus MPa
L	65.98 ±18.24	3.15 ±0.36	27.84 ±8.14
L-MWCNTS 0.1 wt%	38.09 ±6.31	2.91 ±026	16.29 ±2.93
L-MWCNTs 0.5 wt%	28.88 ±6.55	2.65 ±0.33	14.30 ±2.44
L-MWCNTs 1.0 wt%	32.40 ±6.49	2.96 ±0.22	14.07 ±1.81

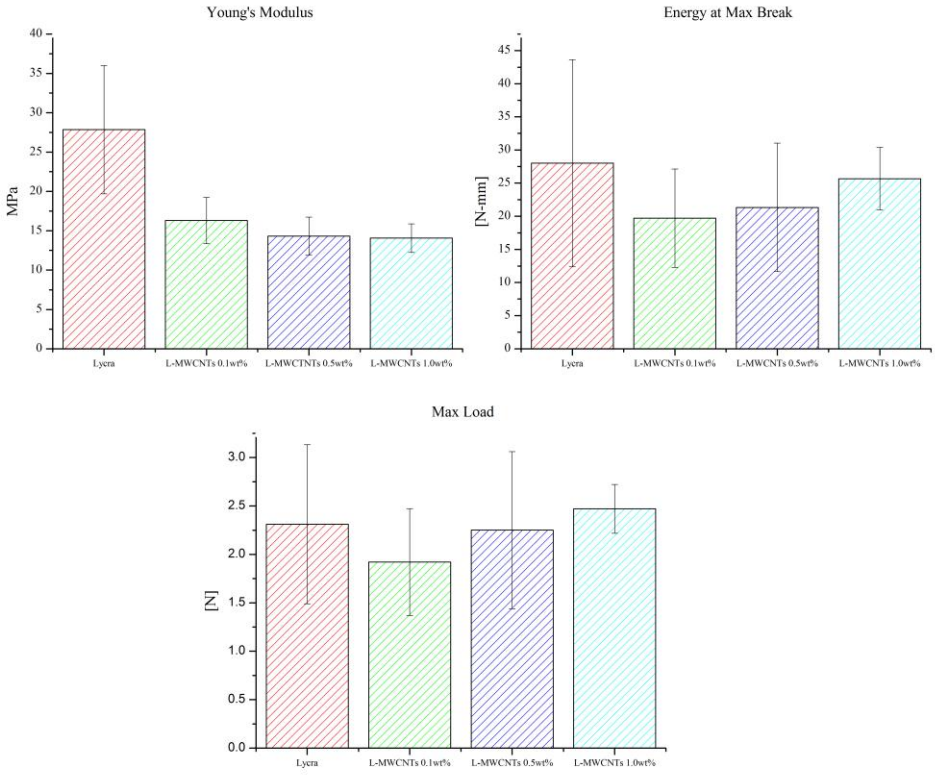

Figure 11 S.D. bar graphs of Lycra®

Table 3 Bar graph values (L)

Polymer	Young's Modulus MPa	Energy at Max Load N-mm	Max Load N
L	27.84 ±8.14	27.99±15.63	2.31 ±0.82
L-MWCNTS 0.1 wt%	16.29 ±2.93	19.72 ±7.41	1.92 ±0.55
L-MWCNTs 0.5 wt%	14.30 ±2.44	21.34 ±9.68	2.25 ±0.81
L-MWCNTs 1.0 wt%	14.07 ±1.81	25.68 ±4.72	2.47 ±0.25

3.2.5 Mechanical Testing

The tensile results for pure Lycra® show a tensile stress of 65.98MPa ±18.24, a strain of 3.15mm/mm±0.36 and the E' of 27.85MPa ±8.14. As the concentration of CNTs increases, the E' decreases reaching a low at L-MWCNTs 1.0 wt% with E' of 13.83MPa. Furthermore, as the MWCNTs were added, the stress and the strain also decreased, finding that among the three samples, the L-MWCNTs 0.1 wt% showed the smaller detriment in mechanical properties. This decrease may be due to many factors, one in of which includes the CNTs not being dispersed properly and thus weakening the polymers structure[19] Based on the TEM images bundiling of the MWCNTs were visible. Also, from the TEM images it is observed that some MWCNTs are protruding out of the polymer matrix, and this deformation may also play a role in the decrease of tensile strength. It was reported that MWCNTs protruding out of the polymer matrix did not break after strained, rather the polymer was broken before the MWCNTs could take over[31]. Another possibility is that the CNTs are being dispersed, but when they are embedded in the polymer matrix they increase the mechanical property to a threshold level lower than L-MWCNTs 0.1 wt%, but when the MWCNTs concentration exceeds this point, the mechanical properties are lowered. If this is the case we are disrupting the crystalline structure of Lycra® and therefore decreasing the mechanical properties of the composites. Based on the results observed in the Raman spectroscopy, the MWCNTs are not dispersed evenly among the polymer at higher concentrations of MWCNTs. By broadening of the G-band, it is shown that the CNTs are not dispersed well enough in the polymer matrix

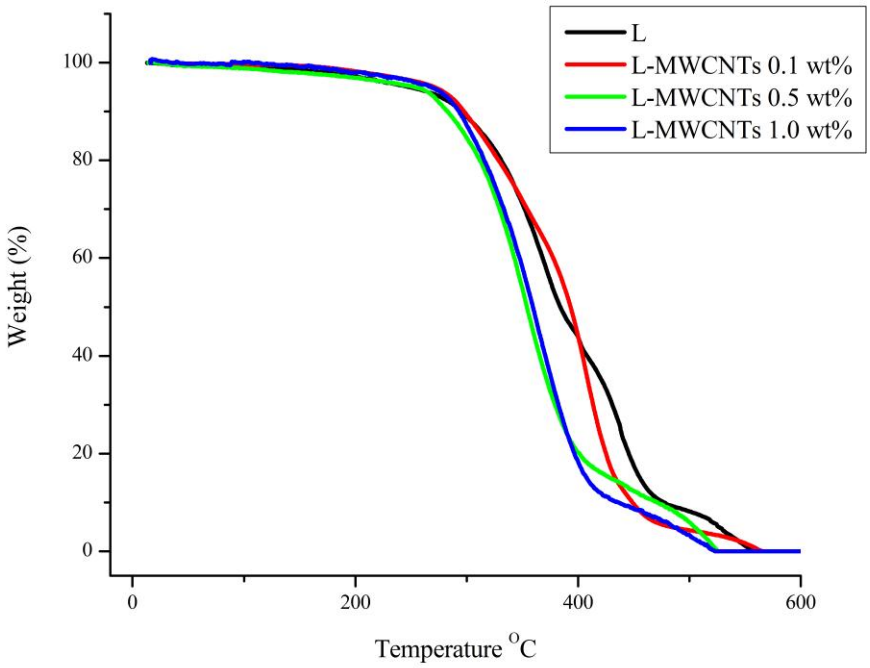

Figure 12 L TGA results

Table 4 Onset Decomposition Temperature for electrospun (L) nanofibers.

Polymer	Onset Decomposition Temp (°C)
Lycra®	303.02
L-MWCNTs 0.1 wt%	293.73
L-MWCNTs 0.5 wt%	302.39
L-MWCNTs 1.0 wt%	299.73

3.2.6 TGA

The TGA result of Lycra® show a decrease of the onset temperature for the polymer nanocomposites. In Table 4, a decrease of 10 °C was the most significant change in the thermal tests, the two other concentrations of 0.5 and 1.0 wt% show a less significant decreased onset temperature ranging 1-4 °C. The decreased onset temperature may be attributed to a lack of adequate dispersion and alignment of the MWCNTs in the polymer matrix[19].

3.3 HydroThane™ (Hyd)

3.3.1 SEM Images

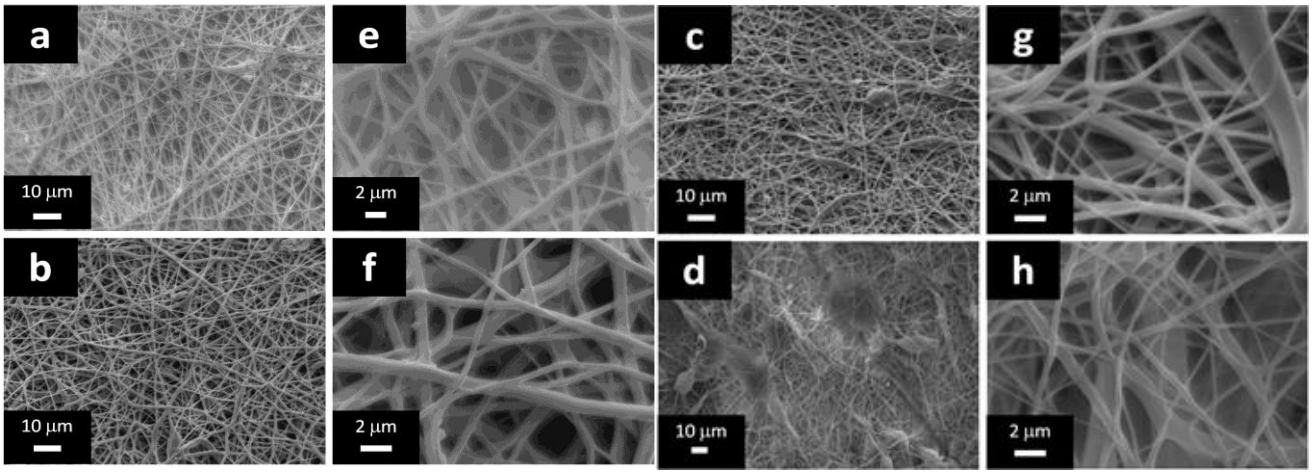

Figure 13 HydroThane at different concentrations at high and low magnification. (a).Hyd, (e) Hyd, (b) Hyd-MWCNTs 0.1 wt%, (f) Hyd-MWCNTs 0.1 wt%, (c) Hyd-MWCNTs 0.5 wt%, (g) Hyd-MWCNTs 0.5 wt%, (d) Hyd-MWCNTs 1.0 wt%, (h) Hyd-MWCNTs 1.0 wt%

Images a & e in Figure 13 are of Hyd nanofibers, demonstrating very little beading and very little agglomeration. Images b-h in Figure are of Hyd nanocomposites with different concentrations of MWCNTs. It has been reported that as the concentration of MWCNTs increases the beading decreased[38]. However, based on our results it is seen that as the MWCNTs concentration increases, beading develops. This beadin may be due to the MWCNTs conductive properties or due to bundling of the MWCNT[18]. When electrospinning, the MWCNTs may be charged and directed to collect in a certain area forming MWCNTs bundles and beading. These results give an indication that the concentration of MWCNTs may be too high at 1.0wt%. In all of the SEM images the fibers are randomly aligned.

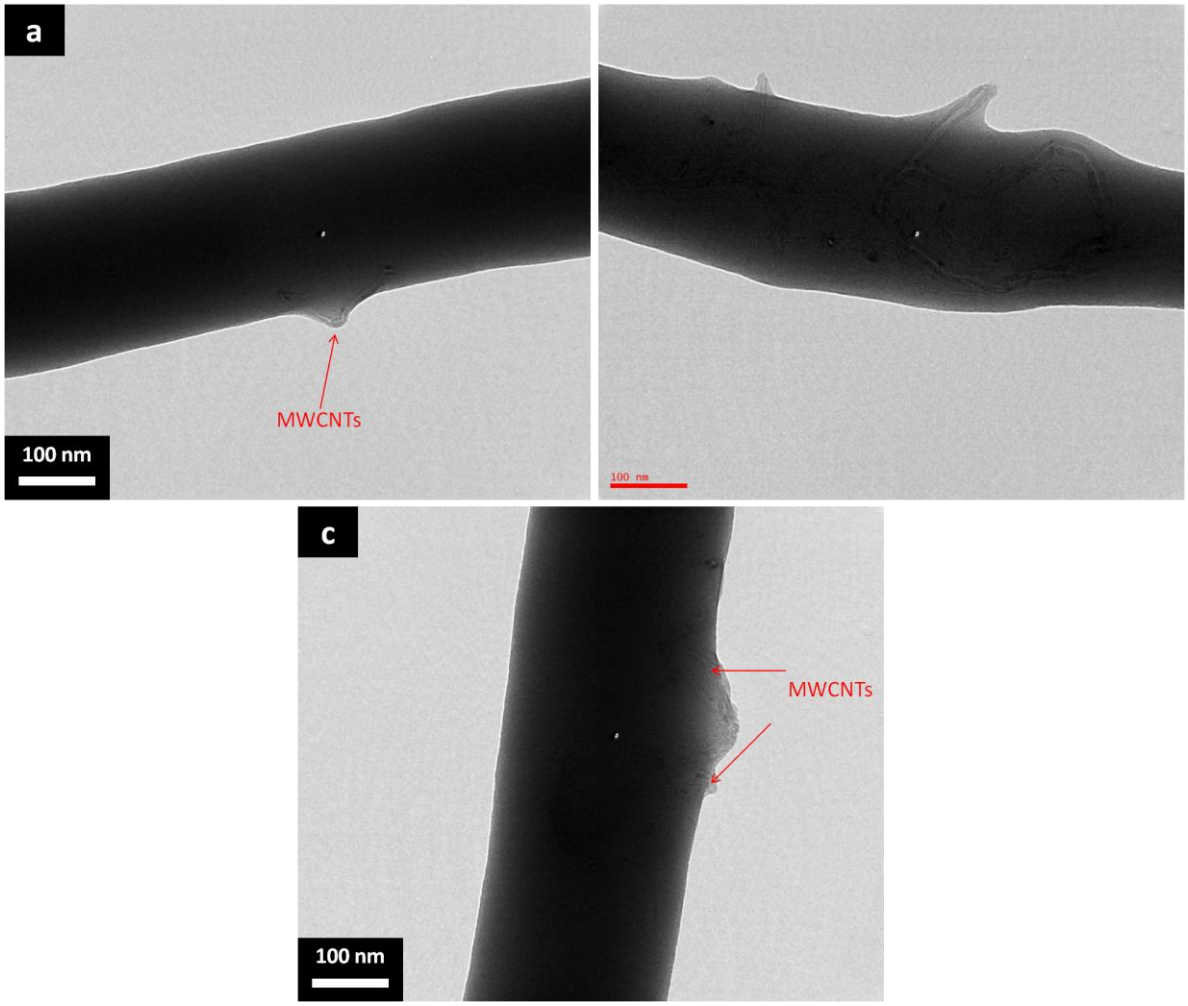

Figure 14 The TEM images are from Hyd-MWCNTs 1.0 wt% in all the images CNTs are protruding from the polymers matrix

3.3.2 TEM Images

The TEM images in Figure 14 are of Hyd-MWCNTs 1.0 wt%, the images show some MWCNTs protruding from the polymers matrix. Compared to the L and Bio, very little bundling is visible. This may explain the higher mechanical properties observed at higher concentrations. The protruding MWCNTS may also help explain the very weak thermal properties observed at this concentration.

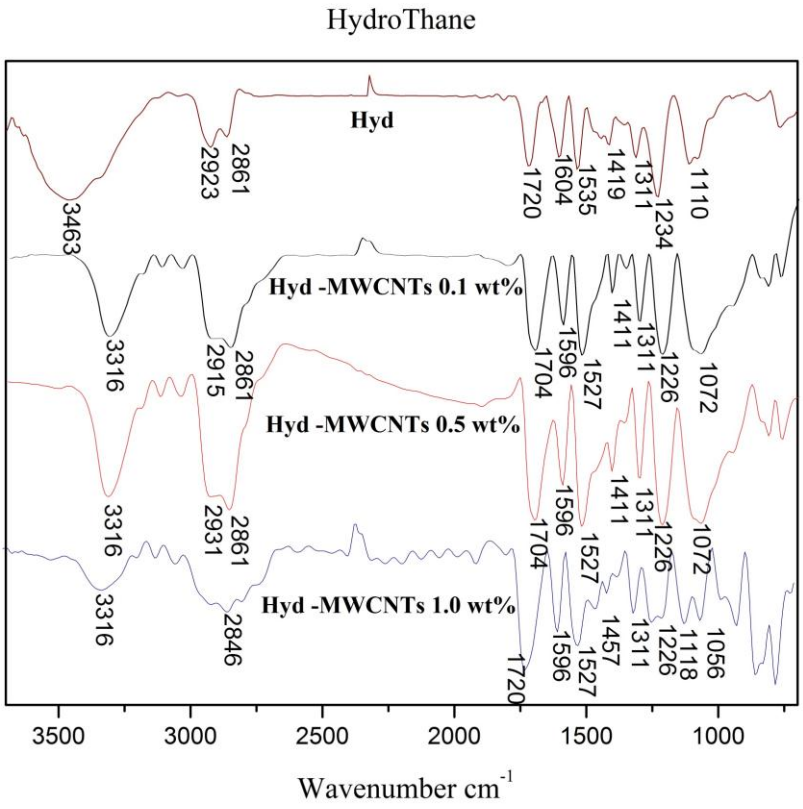

Figure 15 FTIR spectra of Hyd and Hyd nanocomposites

3.3.3 FTIR Spectroscopy

The FTIR of spectra in Figure 15 of electrospun Hyd exhibits a broad band at 3463cm^{-1} due to –OH stretching, 2963cm^{-1} and 2893cm^{-1} stretching due to aliphatic C-H stretches methylene and ethylenediamine[32]. A strong peak at 1720 cm^{-1} is due to N-C=O urethane band at 1640 cm^{-1} is from N-C=O urea band, the band at 1535cm^{-1} is due to N-H in-plane bending. Bands at1226 cm^{-1} and 1110 cm $^{-1}$ attributed to OCONH and C-O-C stretching respectively, which are characteristic bands of the urea and urethane groups[32,33]. In the case of electrospun HydroThane^{TM} containing MWCNTs, the –OH band that was observed in Hyd sample is no longer present. As we examine the OH band there is a slight shoulder that is due to the N-H

band. The N-H band becomes prominent in the samples containing MWCNTs due to the disruption of the H-bonding of the OH present in Hyd. There is a shift in the N-C=O band from 1720cm^{-1} to 1704cm^{-1}, 1704cm^{-1} and 1720cm^{-1} for 0.1 wt% 0.5 wt% and 1.0 wt% respectively. The down shift of 16 wavenumbers is very significant and indicates that the N-C=O is interacting with the MWCNTs this interaction is due to π-π stacking which is similar to what is observed in Lycra®. The fact that the band then shifts back to the position of the pure polymer indicates that the MWCNTs and the polymer may not be interacting with each other, rather the concentration of the MWCNTs so high that the MWCNTs are only interacting with each other and are scattered in bundles in the polymer matrix. There is a shift also in N-C=O and C-O-C bands. The N-C=O bands for 0.1% 0.5% and 1.0% are 1596cm^{-1} 1604cm^{-1}, and 1596cm^{-1}. The O=C-O bands for 0.1%, 0.5%, 1.0% shifts from 1234 cm^{-1}, to 1226cm^{-1} these shifts are also be due to π-π stacking interactions.. The C-O-C band shifts from 1110cm^{-1} to 1072 cm^{-1} in 0.1wt% and 0.5wt%, and in 1.0wt% the band is shifted and split. This shows that the polymer is interacting with the MWCNTs. All of the shifts observed in the FTIR conclude that the polymer and MWCNTs are interacting and the interaction that is most likely accruing is π-π stacking due to the sp^2 properties of the MWCNTs and the nature of the polymers rigid segment.

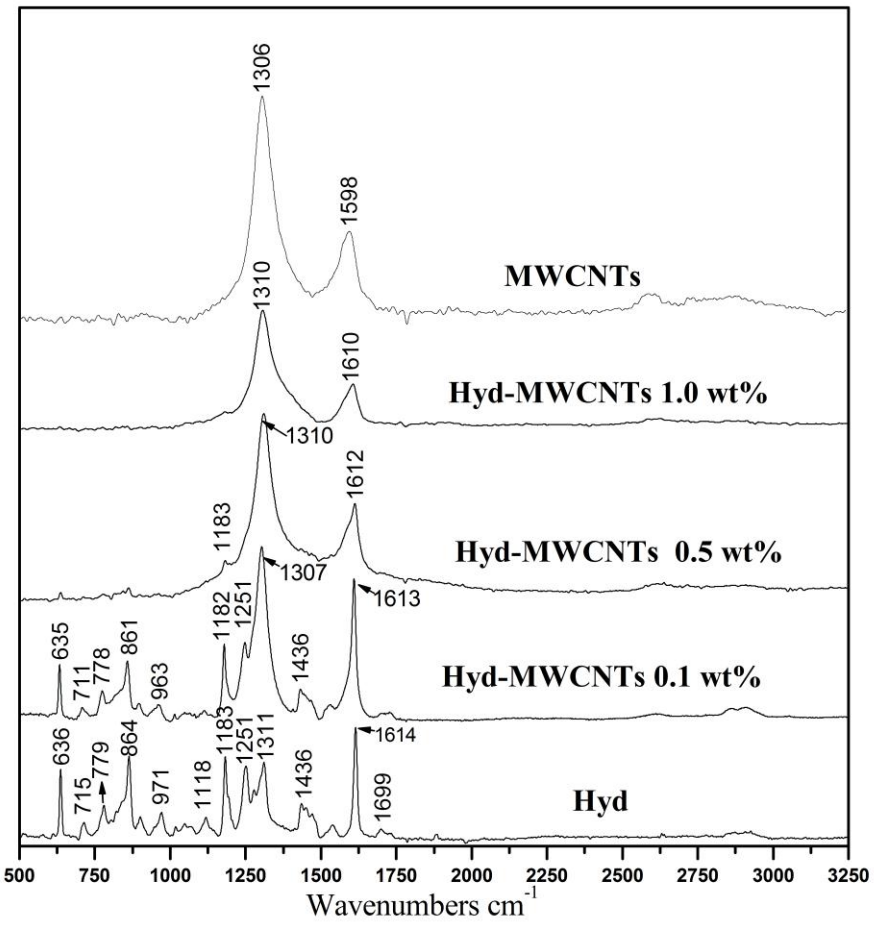

Figure 16: Raman Spectroscopy of Hyd and Hyd-MWCNTs

3.3.4 Raman Spectroscopy

The Raman results in Figure 16 of pure electrospun Hyd show a strong peak at 1614 cm^{-1}, which is due to the C=C of the aromatic ring; peaks at 1251 cm^{-1} and 1183 cm^{-1} are due to C-N stretching and C-O-C stretching respectively. The band at 1435cm^{-1} is attributed to C-H stretching. In the case of Hyd-MWCNTs 0.1wt%, a strong peak at 1307cm^{-1} emerges, being assigned to the tangential D-band which is characteristic of CNTs in general; furthermore this peak is also seen in the samples containing 0.5wt% and 1.0wt% but is shifted to 1310cm^{-1} in both cases[34], this is similar to what is observed in Lycra®.. It is suggested that an up-shift is of the D-band is related to increasing tube diameter and therefore a higher amount of bundling[34,37].

However, it is important to note that these observations were reported for SWCNTs and not MWCNTs. It is noted that since MWCNTs contain an ensemble of carbon nanotubes ranging in diameters that most characteristic trends seen in SWCNTs may not be followed by MWCNTs[37]. Another characteristic of CNTs is known as the G-band, which is observed in the 1600cm^{-1} range[34]. The G-band is observed in Hyd-MWCNTs 0.1wt. %, 0.5% wt.,and 1.0% wt.at 1613cm^{-1}, 1612cm^{-1}, and 1610cm^{-1} respectively. The intensity of the D-band is higher than the G-band in MWCNTs due to the multiple walls of the CNTs[34].As observed in Lycra®, the G-band broadens, being this effect related to the dispersion of MWCNTs in the polymer matrix[34].

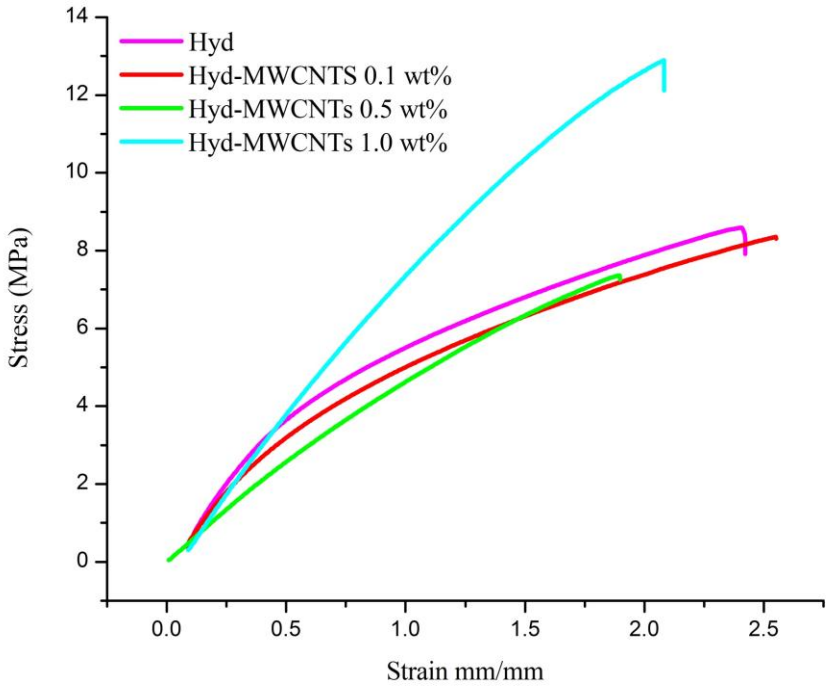

Figure 17 Hyd stress over strain curve

Table 5 Mechanical Results (Hyd)

Polymer	Tensile Stress MPa	Strain mm/mm
Hyd	11.56 ±2.93	2.66 ±0.24
Hyd-MWCNTS 0.1 wt%	8.44 ±0.81	2.61 ±0.12
Hyd-MWCNTs 0.5 wt%	7.78 ±0.83	2.03 ±0.07
Hyd-MWCNTs 1.0 wt%	13.22 ±2.5	2.16 ±0.16

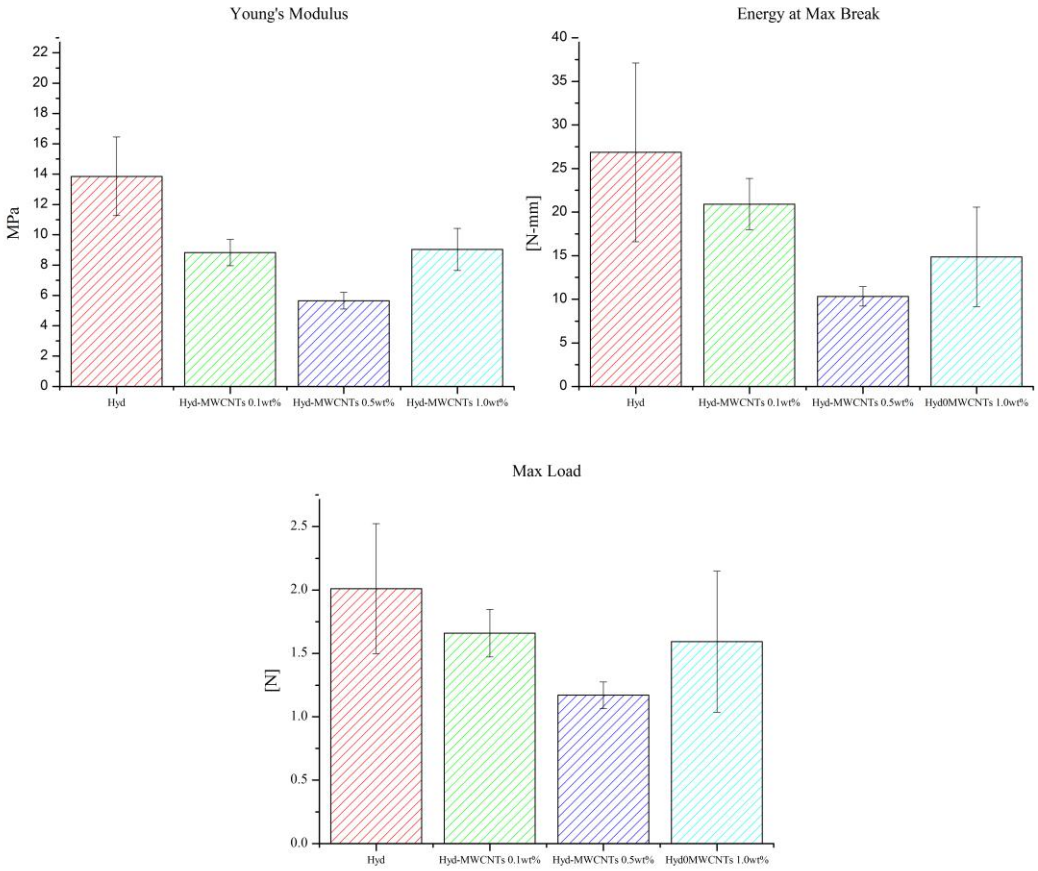

Figure 18 Hyd. S.D. bar graphs

Table 6 Hyd Bar graph values.

Polymer	Young's Modulus MPa	Energy at Max Break N-mm	Max Load N
Hyd	13.86 ±2.59	26.85 ±10.24	2.01 ±0.51
Hyd-MWCNTS 0.1 wt%	8.83 ±0.86	20.92 ±2.93	1.65 ±0.18
Hyd-MWCNTs 0.5 wt%	5.65 ±0.55	10.33 ±1.11	1.16 ±0.10
Hyd-MWCNTs 1.0 wt%	9.03 ±1.38	14.86 ±5.69	1.59 ±0.55

3.3.5 Mechanical Testing

The values form Table 6, show Hyd having a E' of 13.825MPa ±2.59, it is observed from the data that the E' value is decreased at 0.1wt% and 0.5wt and a slight increase at the 1.0wt%. Decrease of the E' value means the polymer is becoming more elastic which in turn means the stiffness is decreasing. The increase of the E' value from the 0.5wt% to 1.0wt% maybe due to the lack of interactions between the polymer and the MWCNTs. From the FTIR data it was concluded that the MWCNTs may not be interacting with the polymer, therefore during the tensile test the bundled MWCNTs and the crystalline of the polymer not as disrupted as in 0.5wt% may have helped increase the E' value. We see this same trend of decreasing initially and then increasing in the highest concentration. Hyd compared to Hyd-MWCNTs 1.0wt% a slight increase in the mean of the stress value, from 11.66MPa ±2.93 to 13.22 ±2.5. Although this may seem significant the S.D. shows that the samples are the same, meaning that the MWCNTs are not affecting the polymer at high concentration. Though the data shows that Hyd and Hyd-MWCNTs 1.0wt% are the same the curve of Hyd-MWCNTs 1.0% shows less deformation than that of the lower concentrations and Hyd. This is observed by a a slight bend in the curve due to deformation of the polymer[39], showing that the MWCNTs are helping the polymer from deforming when strained, which could be an attractive feature when looking for a ligament prosthetic. The energy at max load decreased as the concentration of MWCNTs

increased, this is due to the MWCNTs affecting the crystallinity of Hyd therefore less energy is required to break the polymer. . In the case of Hyd-MWCNTs 0.1 wt%, there is a decrease in the E' and in the stress, the E' was calculated to be 8.0127MPa and the stress decreased to 8.1293MPa. This was also the case with Hyd-MWCNTs 0.5 wt%, the E' decreased to 5.5629MPa. The energy at max break decreases as the MWCNTs concentration increases, though based on the statistical data the results are not significant. It is concluded that the MWCNTs did not affect the energy at break.

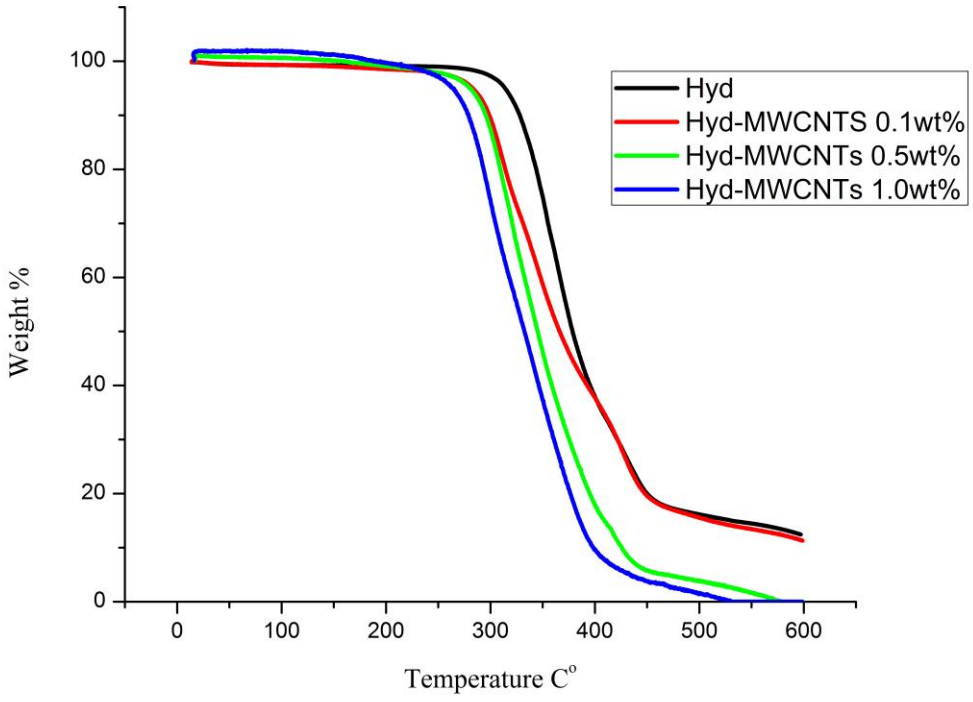

Figure 19 Thermal Gravimetric Analysis of Hyd nanofibers

Table 7 Onset decomposition temperature of electrospun Hyd fiber

Polymer	Onset Decomposition Temp (^{o}C)
Hyd	324.92
Hyd-MWCNTs 0.1 wt%	285.04
Hyd-MWCNTs 0.5 wt%	287.44
Hyd-MWCNTs 1.0 wt%	269.59

3.3.6 TGA

The TGA results of electrospun Hyd showed a decomposition point at 342.92 ^{o}C. In the case of the samples that contained MWCNTs, the decomposition point decreased in all samples. Hyd-MWCNTs 1.0 wt.% decreased the most by 55^{o}C to 269.59^{o}C, followed by Hyd-MWCNTs 0.1 wt.% to 285^{o}C, and Hyd-MWCNTs 0.5 wt. % to 287^{o}C. There are many factors that may have affected this onset decomposition temperature one , being an uneven dispersion of MWCNTs in the polymer matrix[19] a possibility, causing heat transfer to uneven distribution along the sample, so certain areas may have degraded at an earlier onset temperature.

3.4 BioSpan®(Bio)

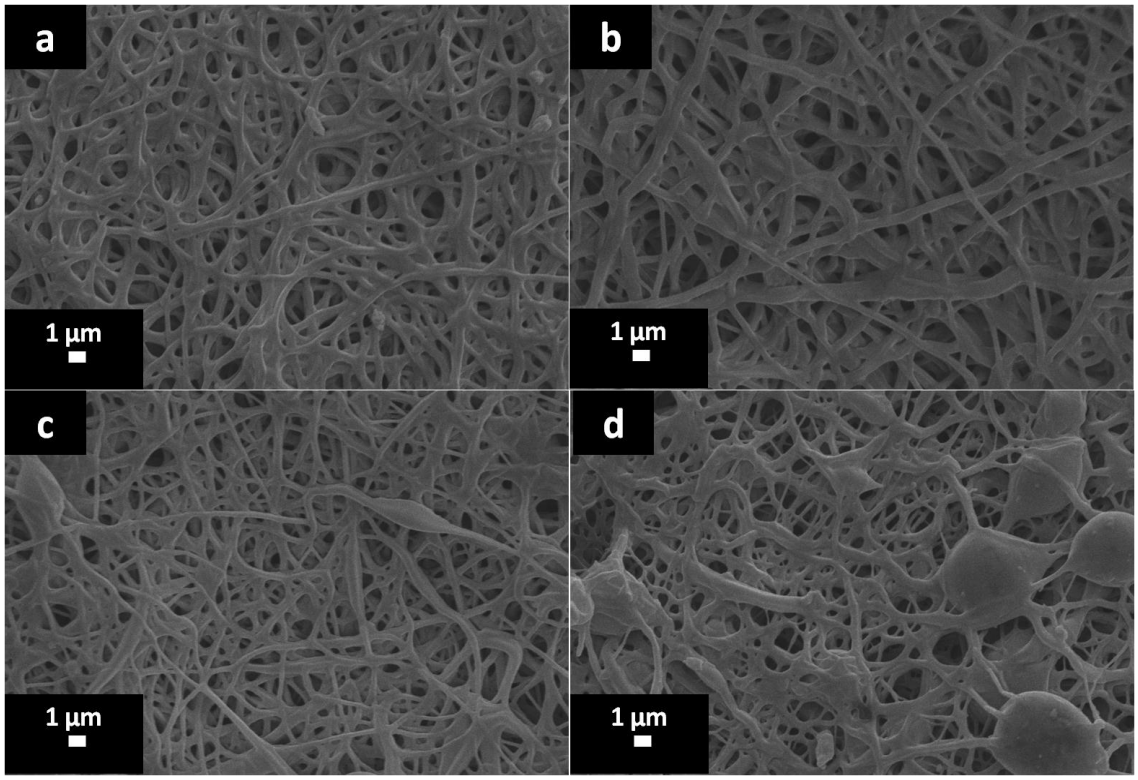

Figure 20 SEM images of BioSpan® (Bio). (a) electrospun Bio, (b) Bio-MWCNTs 0.1 wt%, (c) Bio-MWCNTs 0.5 wt%, (d) Bio-MWCNTs 1.0 wt%

3.4.1 SEM Images

From Figure 20, the SEM images show that all the samples are electrospun with random alignment; as the concentration of the MWCNTs increases, more beading is observed. As seen in image (d), there is a high amount of beading. This may be attributed to the MWCNTs conductive properties when electrospinning, this was reported in previous work done by our lab in the case of polystyrene and CNTs, and this beading is also visible in Hyd[38]. This beading may have an effect on the mechanical properties of this polymer.

3.4.2 TEM Images

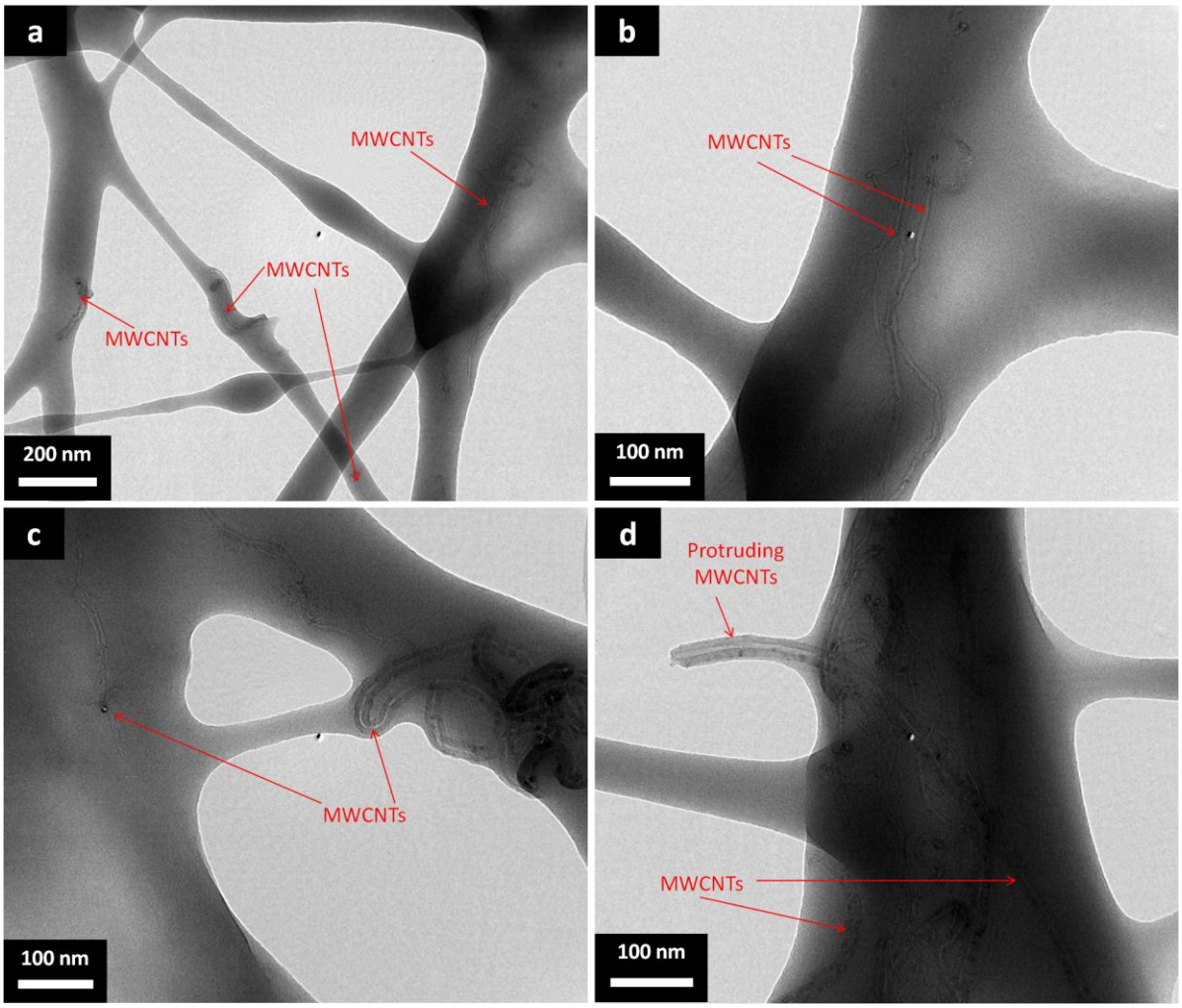

Figure 21 TEM images of Bio-MWCNTs 1.0 wt%.

The TEM images of Figure 21 show clearly that the CNTs are present randomly in the polymer matrix. In image (a), there seems to be a cluster of CNTs inside the polymer matrix, and in image (d) a nanotube is protruding out of the polymer matrix. In image (c), another cluster of MWCNTs is also visible. This was also seen in L TEM images.

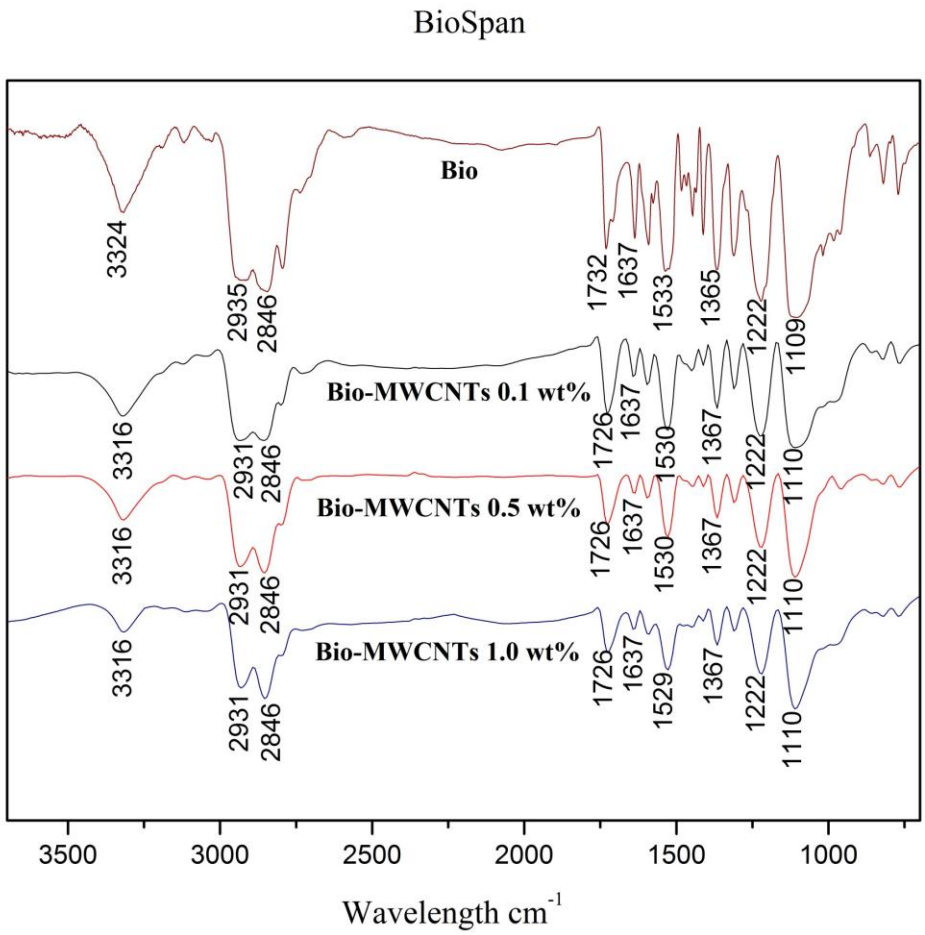

Figure 22 FTIR spectra of BioSpan® electrospun.

3.4.3 FTIR Spectroscopy

The FTIR spectrum from Figure 22 show characteristic bands of PUs, the N-H peak is shown at 3324cm^{-1}, the N-C=O band of urethanes is present at 1732 cm^{-1}, the 1637 cm^{-1} band represents N-C=O from the urea group and the band at 1100cm^{-1} is attributed to C-O-C bond[33,32]. From Figure , samples that contain MWCNTs show certain shifts in some of these bands. The N-H band is shifted down from 3324 to 3316cm^{-1} once the MWCNTs are added this is a results of an interaction with the MWCNTs and the polymer. It is also observed that the C-H peak intensities at 2935 and 2846 cm^{-1} differ from sample to sample. A change in intensity is a result of a change in dipole moment so from the interactions between the polymer and the MWCNTs there is an

increase in C-H asymmetric bending. The band at 2935 cm^{-1} is shifted downward to 2931 cm^{-1} when the MWCNTs are introduced. The N-C=O band at 1732 cm^{-1} is also down shifted once the MWCNTs are introduced this is due to the π-π interaction between the MWCNTs pi electrons and the urethane groups pi electron. The N-C=O band at 1637 cm^{-1} does not shift but weakens in intensity and this is due to less of a dipole moment change. The band at 1533 cm^{-1} is attributed to N-H bending; this band down shifts as the concentration of MWCNTs increases. These shifts are due to interactions between the polymer and MWCNTs. The bands at 1222 and 1100 cm^{-1} are attributed toOCONH and C-O-C bonds respectively. The ether band narrows as the concentration of MWCNTs is increased, this may be due to the MWCNTs not allowing the band to bend as freely compared to the sample that does not contain MWCNTs, and this is also observed in Lycra®.

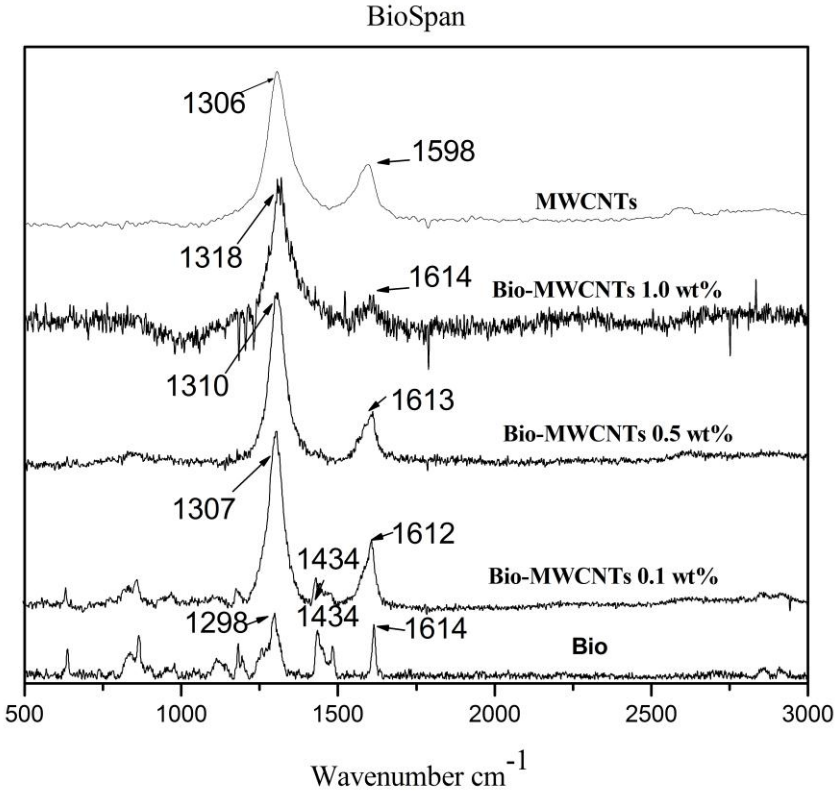

Figure 23: Raman spectroscopy of Bio and Bio-MWCNTs MWCNTs raman

3.4.4 Raman Spectroscopy

The Raman spectra in Figure 23 shows characteristic bands of the polymer. The band at 1614 cm^{-1} and 1434 cm^{-1} are due to C=C aromatic rings the band at 1298 cm^{-1} is from aromatic ethers. Once the MWCNTs are introduced the bands are shifted. The band at 1614 cm^{-1} is shifted to 1612 cm^{-1} in the sample Bio-MWCNTs 0.1wt%, this is the G-band a characteristic band mentioned previously in Lycra® and HydroThane™. As observed before with Lycra® and HydroThane™, the G-band narrows as the MWCNTs concentration increases, which is related to the dispersion of the MWCNTs in the polymer. As the concentration of MWCNTs increases, the band at 1434 cm^{-1} vanishes this may be due to masking of the polymer by the MWCNTs. The band at 1298cm^{-1} is shifted to the 1300cm^{-1} range. This is from the characteristic D-band which was also visible in Lycra® and HydroThane™.

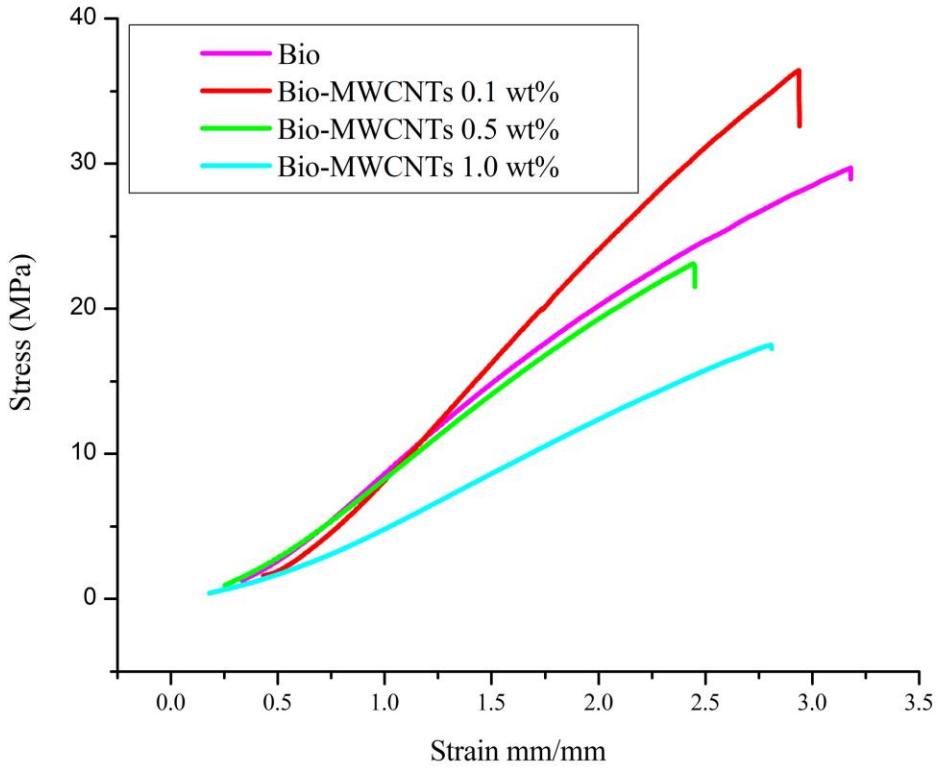

Figure 24 Stress over Strain curve for Bio.

Table 8 Mechanical results for Bio

Polymer	Tensile Stress MPa	Strain mm/mm
Bio	29.01 ±12.01	2.95 ±0.60
Bio-MWCNTS 0.1 wt%	40.44 ±8.83	3.29 ±0.26
Bio-MWCNTs 0.5 wt%	26.22 ±7.65	2.71 ±0.17
Bio-MWCNTs 1.0 wt%	20.07 ±2.89	2.98 ±0.07

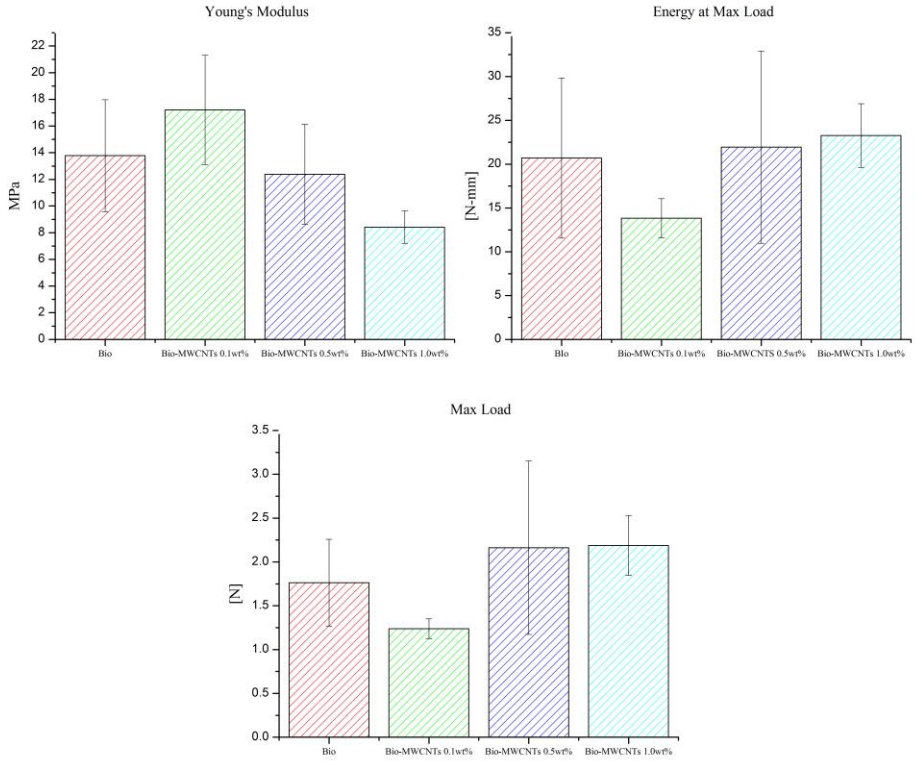

Figure 25 Bio S.D. bar graphs

Table 9 Bio Bar graph values

Polymer	Young's Modulus MPa	Energy at Max Break N-mm	Max Load N
Bio	13.78 ±4.2	20.68 ±9.14	1.76 ±0.49
Bio-MWCNTS 0.1 wt%	17.21 ±4.1	13.83 ±2.22	1.24 ±0.11
Bio-MWCNTs 0.5 wt%	12.39 ±3.7	21.94 ±10.97	2.19 ±0.99
Bio-MWCNTs 1.0 wt%	8.42 ±1.2	23.26 ±3.62	2.18 ±0.34

3.4.5 Mechanical Testing

The mechanical stresses over strain curves show mechanical improvement for Bio-MWCNTS 0.1wt%. However, samples with a higher concentration of MWCNTs demonstrated weaker mechanical properties. This may be due to the MWCNTs disrupting the polymer matrix to a point where it is weakened. The E' for electrospun Bio was 13.78 MPa ± 4.2, which was increased to 17.21 MPa ±4.1 for Bio-MWCNTs 0.1wt%. The E' was decreased in the samples containing higher concentration of MWCNTs. This is due to the the MWCNTs disrupting the crystillinity of the polymer and in turn lowering the stiffness of the polymer. The energy at max break does not show a significant difference from the samples containing MWCNTs, the S.D. falls in the mean of all of the samples so statistically the values are the same.

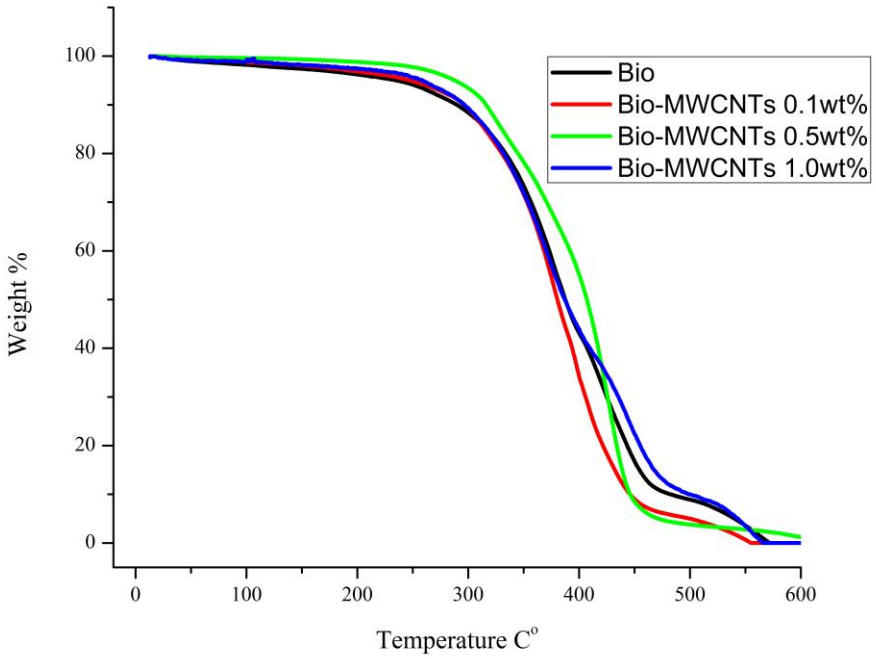

Figure 26 Bio TGA

Table 10 Bio TGA onset Temp data

Polymer	Onset Decomposition Temp (^{o}C)
Bio	322.01
Bio-MWCNTs 0.1 wt%	329.90
Bio-MWCNTs 0.5 wt%	340.02
Bio-MWCNTs 1.0 wt%	311.56

3.4.6 TGA

The data observed in Table 10 shows that the onset temperature increased in Bio-MWCNTs 0.1wt% and Bio-MWCNTs 0.5wt% , this is due to the nature of MWCNTs dispersed in the polymer matrix. It is seen in Table 10 Bio-MWCNTs 1.0wt% onset temperature decreases this may be due to inadequate dispersion of the MWCNTs in the polymer matrix[38]. This indicates that a threshold may have been met and concentration higher than 1.0wt% in Bio will not be suitable in increasing the thermal properties.

CHAPTER IV

CONCLUSION

Three commercially available PUs were successfully electrospun into nanofibers and confirmed by SEM. Addition of MWCNTs however showed from mechanical testing and thermal tests that the MWCNTs did not improve Lycra® and HydroThane™. In the case of BioSpan® a slight improvement in the mechanical properties was observed and in the thermal properties. The TEM images, FTIR and Raman spectroscopy confirmed the presence of the MWCNTs in the polymer matrix. In addition, TEM images showed MWCNTs protruding out of the polymer in all three polymer matrices. These tests lead to the conclusion that the process of incoorperating the MWCNTs needs to be modified to decrease bundling of the. From the SEM images, for the exception of Lycra® beading and clumping was observed especially in BioSpan® , this is due to the MWCNTs electrical properties and the electrospinning method, due to the high concentration of MWCNTs in the polymer matrix it can be predicted that the charge created may have led to the MWCNTs attracting to each other forming bundles. The mechanical tests for the three PUs showed different results for all. It is concluded that the MWCNTs are weakening Lycra® in general. A different method may be used to incorporate the MWCNTs in to Lycra®, perhaps modifying the MWCNTs so they attach better to the polymer may yield better results. In the case of HydroThane™ the highest E' value was of Hyd, but the highest strain was Hyd-MWCNTs 1.0 wt%. The MWCNTs appeared to keep Hyd-MWCNTs 1.0 wt% from deforming as shown in the lower concentration and the pure polymer. Perhaps the threshold has not been reached and a higher concentration of MWCNTs will yield better

mechanical results. In the case of BioSpan®, the sample with the highest E' was Bio-MWCNTs 0.1 wt%; from the results, it is possible that the higher concentration could also show promising results if the beading formed while electrospinning is controlled. It is difficult to say that the MWCNTs weakened the polymer without neglecting the fact the beading of the sample will really affect the mechanical results. The Thermal results for the polymers were not as expected, theoretically if the MWCNTs are dispersed correctly in the polymer matrix then the onset temperature should increase .based on the thermal properties of the MWCNTs. In both HydroThane™ and Lycra®, the MWCNTs lowered the onset decomposition temperature. These results may be attributed to MWCNTs bundling in the polymer matrix. In the case of BioSpan® the onset temperature was increased in samples Bio-MWCNTs 0.1wt% and Bio-MWCNTs 0.5wt%.

4.1 Future Research

There is still much work that needs to be done. Further tests should be done on the degree of MWCNTs dispersion within the polymer matrix, since there are many methods that help functionalize CNTs to enhance the interaction between the polymer and CNTs.. The possibility of uniformly aligning these polymers by use of the electrospinning method may help improve the mechanical properties and thermal stability of these samples. BioSpan® and HydroThane™ both showed the possibility of being improved by the use of MWCNTs, adjustment to some parameters from this experiment may help improve them. The capability of PUs being used as ligament prosthetics is still a reality and can be achieved with further experiments and time.

REFERENCES

(1) POLYURETHANE http://www.sdplastics.com/polyuret.html.

(2) Gary T. Howard *International Biodeterioration & Biodegradation* **2002**, *49*, 245–252.

(3) Huang, Z.-M.; Zhang, Y.-Z.; Kotaki, M.; Ramakrishna, S. *Composites Science and Technology* **2003**, *63*, 2223–2253.

(4) Clemitson I.R *Castable Polyurethanes Elastomers*; Group, T. & F., Ed.; Florida, 2008.

(5) T, T. *Polyurethanes as Specialty Chemicals: Principles and Applications*; CRC Press: Florida, 2005.

(6) Weitz, R. T.; Harnau, L.; Rauschenbach, S.; Burghard, M.; Kern, K. *Nano letters* **2008**, *8*, 1187–91.

(7) Ellison, C. J.; Phatak, A.; Giles, D. W.; Macosko, C. W.; Bates, F. S. *Polymer* **2007**, *48*, 3306–3316.

(8) Medeiros, E. *Journalof Applied Polymer Science* **2009**, *113*, 2322–2330.

(9) Teo, W. E.; Ramakrishna, S. *Nanotechnology* **2006**, *17*, R89–R106.

(10) Huang, Z.-M.; Zhang, Y.-Z.; Kotaki, M.; Ramakrishna, S. *Composites Science and Technology* **2003**, *63*, 2223–2253.

(11) Yao, L.; Haas, T.; Guiseppi-Elie, A. *Chemistry of Materials* **2003**, *15*, 1860–1864.

(12) merriam-webster http://www.merriam-webster.com/.

(13) Knee Conditions Orthopaedic & Neurosurgery Specialists . http://www.onsmd.com/knee/.

(14) Sachlos, E.; Czernuszka, J. T. *European cells & materials* **2003**, *5*, 29–39; discussion 39–40.

(15) Khaled, E. G.; Saleh, M.; Hindocha, S.; Griffin, M.; Khan, W. S. *The open orthopaedics journal* **2011**, *5 Suppl 2*, 289–95.

(16) Salvetat, J.-P.; Bonard, J.-M.; Thomson, N. H.; Kulik, A. J.; Forró, L.; Benoit, W.; Zuppiroli, L. *Applied Physics A: Materials Science & Processing* **1999**, *69*, 255–260.

(17) Salvetat-Delmotte, J. *Carbon* **2002**, *40*, 1729–1734.

(18) Dirk M. Guldi, N. M. *Carbon Nanotubes and Related Structures: Synthesis, Characterization, Functionalization, and Applications*; Dirk M. Guldi, N. M., Ed.; John Wiley & Sons, 2003.

(19) Jiang, L.; Tan, H.; Wu, J.; Huang, Y.; Hwang, K.-C. *Nano* **2007**, *2*, 139.

(20) Vaisman, L.; Wagner, H. D.; Marom, G. *Advances in colloid and interface science* **2006**, *128-130*, 37–46.

(21) Xie, X.; Mai, Y.; Zhou, X. *Materials Science and Engineering: R: Reports* **2005**, *49*, 89–112.

(22) Thompson, C. J.; Chase, G. G.; Yarin, A. L.; Reneker, D. H. *Polymer* **2007**, *48*, 6913–6922.

(23) Yang, Q.; Li, Z.; Hong, Y.; Zhao, Y.; Qiu, S.; Wang, C.; Wei, Y. *Journal of Polymer Science Part B: Polymer Physics* **2004**, *42*, 3721–3726.

(24) Heikkila, P. *eXPRESS Polymer Letters* **2009**, *3*, 437–445.

(25) Katti, D. S.; Robinson, K. W.; Ko, F. K.; Laurencin, C. T. *Journal of biomedical materials research. Part B, Applied biomaterials* **2004**, *70*, 286–96.

(26) Macossay, J.; Marruffo, A.; Rincon, R. *Polymers for Advanced Technologies* **2007**, *18*, 180–183.

(27) Hajra, M. .; Mehta, K.; Chase, G. . *Separation and Purification Technology* **2003**, *30*, 79–88.

(28) Gigliotti, B.; Sakizzie, B.; Bethune, D. S.; Shelby, R. M.; Cha, J. N. *Nano letters* **2006**, *6*, 159–164.

(29) Cantu, T. 2009 HESTEC POSTER.

(30) Safarova, K.; Dvorak, A.; Kubinek, R. *Modern Research and* **2007**, 513–519.

(31) Bower, C.; Rosen, R.; Jin, L.; Han, J. *Applied Physics Letters* **1999**, *74*, 2–4.

(32) Xiong, J.; Zheng, Z.; Qin, X.; Li, M.; Li, H.; Wang, X. *Carbon* **2006**, *44*, 2701–2707.

(33) Sahoo, N. G. *Journal of the Korean Pysical Society* **2007**, *51*, 1–6.

(34) Jorio, A.; Pimenta, M.; Filho, A. S. *New Journal of Physics 5* **2003**, *139*, 139.1–139.17.

(35) Marucci, A.; Brown, S.; Corio, P.; Pimenta, M. In *AIP Conference*; 2000; pp. 1–15.

(36) Osswald, S.; Havel, M. *Journal of Raman Spectroscopy* **2007**, *38*, 728–736.

(37) Dresselhaus, M. S.; Dresselhaus, G.; Saito, R.; Jorio, A. *Physics Reports* **2005**, *409*, 47–99.

(38) Macossay, J.; Ybarra, A. V. R.; Arjamend, F. a.; Cantu, T.; Eubanks, T. M.; Chipara, M.; López-Cuéllar, E.; Mohamed-Noriega, N. *Designed Monomers & Polymers* **2012**, *15*, 197–205.

(39) Roylance, D. Stress-strain curves, 2001, pp. 1–14.

(40) Lycra® structure http://osf1.gmu.edu/~sslayden/curr-chem/spandex/spandex-prob.htm.

(41) Recovering from ACL Surgery: The Long Road to the Surgery Table http://aclsurgeryrecovery.blogspot.com/2008/05/long-road-to-surgery-table.html.

(42) Functionalised carbon nanotubes as therapeutic vectors http://www-ibmc.u-strasbg.fr/ict/images/SWNT_MWNT.jpg (accessed Jul 11, 2012).

(43) Masiuk, S.; Rakoczy, R. *Chemical Engineering and Processing: Process Intensification* **2009**, *48*, 538–548.

BIOGRAPHICAL SKETCH

Travis Cantu was born in 1987 in McAllen TX. He entered The University of Texas-Pan American in 2005 and began his undergraduate studies. In 2010 he completed his undergraduate studies and continued on to pursue a Master of Chemistry at the University of Texas-Pan American. In 2012 he will enter the Material Science Engineering and Commercialization at Texas State University.

Email address: tcantuy1@utpa.edu